Journal of Medicinal Chemistry

Article

Indolyl Azaspiroketal Mannich Bases Are Potent Anti-mycobacterial Agents with Selective Membrane Permeabilizing Effects and In Vivo Activity

Samuel Agyei Nyantakyi, Ming Li, Pooja Gopal, Matthew Zimmerman, Veronique Dartois, Martin Gengenbacher, Thomas Dick, and Mei-Lin Go

J. Med. Chem., **Just Accepted Manuscript** • DOI: 10.1021/acs.jmedchem.8b00777 • Publication Date (Web): 12 Jun 2018

ACS Publications

is published by the American Chemical Society. 1155 Sixteenth Street N.W., Washington, DC 20036

Indolyl Azaspiroketal Mannich Bases Are Potent Anti-mycobacterial Agents with Selective Membrane Permeabilizing Effects and In Vivo Activity

Samuel Agyei Nyantakyi, [# +] Ming Li, [^ +] Pooja Gopal, [^] Matthew Zimmerman, [§] Véronique Dartois, [§] Martin Gengenbacher, [§] Thomas Dick [* $ §] and Mei-Lin Go, [* #]

Department of Pharmacy, 18 Science Drive 4, National University of Singapore, Singapore 117543; ^ Department of Medicine, 14 Medical Drive, National University of Singapore, Singapore 117599; [$] Department of Microbiology and Immunology, 5 Science Drive 2, National University of Singapore, Singapore 117545; [§] Public Health Research Institute, New Jersey Medical School, Rutgers, The State University of New Jersey, 225, Warren Street, Newark, New Jersey, USA 07 103-2714.

+ Joint first authors

Abstract

The inclusion of an azaspiroketal Mannich base in the membrane targeting anti-tubercular 6-methoxy-1-*n*-octyl-1*H*-indole scaffold resulted in analogs with improved selectivity and submicromolar activity against *Mycobacterium tuberculosis* H37Rv. The potency enhancing properties of the spiro-ring fused motif was affirmed by SAR and validated in a mouse model of tuberculosis. As expected for membrane inserting agents, the indolyl azaspiroketal Mannich bases perturbed phospholipid vesicles, permeabilized bacterial cells and induced the mycobacterial cell envelope stress reporter promoter p*iniBAC*. Surprisingly, their membrane disruptive effects did not appear to be associated with bacterial membrane depolarization. This profile was not uniquely associated with azaspiroketal Mannich bases but was characteristic of indolyl Mannich bases as a class. Whereas resistant mycobacteria could not be isolated for a less potent indolyl Mannich base, the more potent azaspiroketal analog displayed low

spontaneous resistance mutation frequency of 10^{-8}/CFU. This may indicate involvement of an additional envelope-related target in its mechanism of action.

INTRODUCTION

Tuberculosis (TB) has been a scourge for most of history. [1] In spite of advances in our understanding of the pathogenic organism *Mycobacterium tuberculosis* (*Mtb*), TB remains frustratingly difficult to treat and continues to extract a high toll of human lives. In 2016, TB surpassed HIV-AIDS and malaria as the leading cause of death due to a single infectious agent. [2] The past decade has witnessed continuing resistance to first line anti-TB drugs isoniazid and rifampicin (multi-drug resistance), additional resistance to fluoroquinolones and second-line injectables (extensive drug resistance), and more recently, cases of programmatically incurable TB where treatment regimens constructed with available drugs completely fail. [3] Most drugs used today were discovered decades ago and the global TB drug pipeline, notwithstanding recent additions like bedaquiline, remains thin. [4] While the urgency for new drugs cannot be overemphasized, a more compelling need is for agents that kill both replicating and phenotypically drug tolerant nonreplicating populations of mycobacteria. Disrupting the mycobacterial membrane has been posited as a viable means of achieving these objectives. [5] First, the loss of an architecturally intact and functional membrane is fatal to both growing and quiescent bacteria. [5] Second, the ensuing perturbation of multiple membrane-embedded targets would further delay resistance development among surviving organisms. [5] The feasibility of this approach is corroborated by membrane-active small molecules (verapamil, [6] boromycin, [7] amphiphilic xanthones, [8] propyltriphenylphosphonium phenothiazine conjugates, [9] 1-octylindolyl Mannich bases [10]) that have antimycobacterial activity. Involvement of the mycobacterial membrane was inferred from the ability of these compounds to permeabilize mycobacterial membranes, [7, 8, 10] disrupt transmembrane potential [6, 7] and/or deplete intracellular ATP. [7, 8] Tellingly, conjugation of the membrane targeting triphenylphosphonium (TPP) moiety to

antimycobacterial phenothiazines led to significant improvements in activity, likely due to enhanced localization within the mycobacterial membrane.[9] Relatably, grafting TPP onto an inactive indole scaffold resulted in mycobactericidal cationic amphiphilic TPP indoles that rapidly depolarized the membrane of *M. bovis* BCG. [11] 1-Octylindolyl Mannich bases embedded with a cationic amphiphilic motif were similarly mycobactericidal and additionally, more potent and selective than the TPP indoles. [10,11] Among the more potent indolyl Mannich bases, compound **1** (8-[(6-methoxy-1-octyl-1*H*-indolyl-3-yl)methyl]-1,4-dioxa-8-azaspiro[4,5]decane) stood out as the only member with an azaspiroketal side chain (Figure 1). [10] We noted that a structurally similar motif was present in the preclinical TB candidate BTZ043 (**2,** Figure 1). [4, 12] Mechanistically, the azaspiroketal has not been implicated in the potent activity of BTZ043 which was attributed to inhibition of the oxidoreductase DprE1, a key enzyme involved in mycobacterial cell wall synthesis. [13,14] The contribution of the azaspiroketal to the anti-TB activity of BTZ043 remains elusive as structural variations have yielded mixed results. Notably, the antimycobacterial activity of **3** which does not possess a spirocyclic side chain, was comparable to BTZ043 (Figure 1) [15] whereas replacing the ketal oxygens in BTZ043 with sulfur resulted in a more active analog **4** (Figure 1). [16] Spirocyclic motifs are widely perceived to possess attractive attributes from a drug design perspective due to their unique dimensionality and complexity. [17] Evidence from literature has shown that the inclusion of spirocycles in molecules led to tighter and more selective binding to desired targets, improved solubility and greater metabolic stability. [18,19] Viewed in this context and as part of our efforts to optimize the antimycobacterial activity of indolyl Mannich bases, we explored the azaspirocyclic motif with two goals in mind: First, to assess its potential as a potency-enhancing chemotype, and second, to determine if it is associated with distinctive mechanistic effects that set it apart from other Mannich bases.

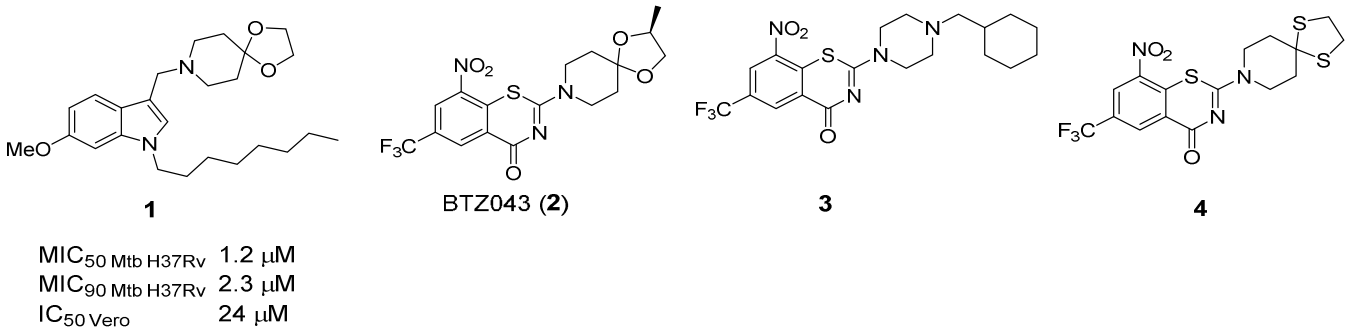

Figure 1: Structures of indolyl Mannich base **1**, BTZ043 (**2**) and its benzothiazinone congeners **3** and **4**

Chemistry

Three series of indolyl Mannich bases were synthesized to interrogate the structure-activity contribution of the spirocyclic motif. In Series 1, diverse azaspirocycles were introduced as the basic moiety at position 3 of the 1-*n*-octyl-6-methoxyindolyl scaffold. We then sought to optimize activity of the more potent Series 1 members by replacing *n*-octyl with ring bearing side chains (Series 2), and introducing alternative substituents (nitro, cyano, propoxy, isopropoxy, benzyloxy) in place of methoxy (Series 3). Also prepared were 1-octylindoles in which the azaspirocycle was not part of the Mannich base motif but attached to indole via an alkoxy linker (Series 4).

Series 1-3 were synthesized by methods previously reported for indolyl Mannich bases. [10] Scheme 1 outlines the synthesis of Series 1 which involves reacting 6-methoxy-1*H*-indole with 1-bromooctane in the presence of sodium hydride to give the 1-(*n*-octyl) analog **5,** followed by the insertion of the basic 3-substituted aminomethyl side chain by two approaches. In the first, the indole-3-carbaldehyde **6** was prepared by a Vilsmeier-Haack reaction and then subjected to reductive amination to give compounds **21, 22, 28 – 32, 35**. In the second

approach, **5** was reacted with an amine and formaldehyde in the presence of an acid catalyst (acetic acid or zinc chloride) to give the remaining Series 1 compounds.

SERIES 1

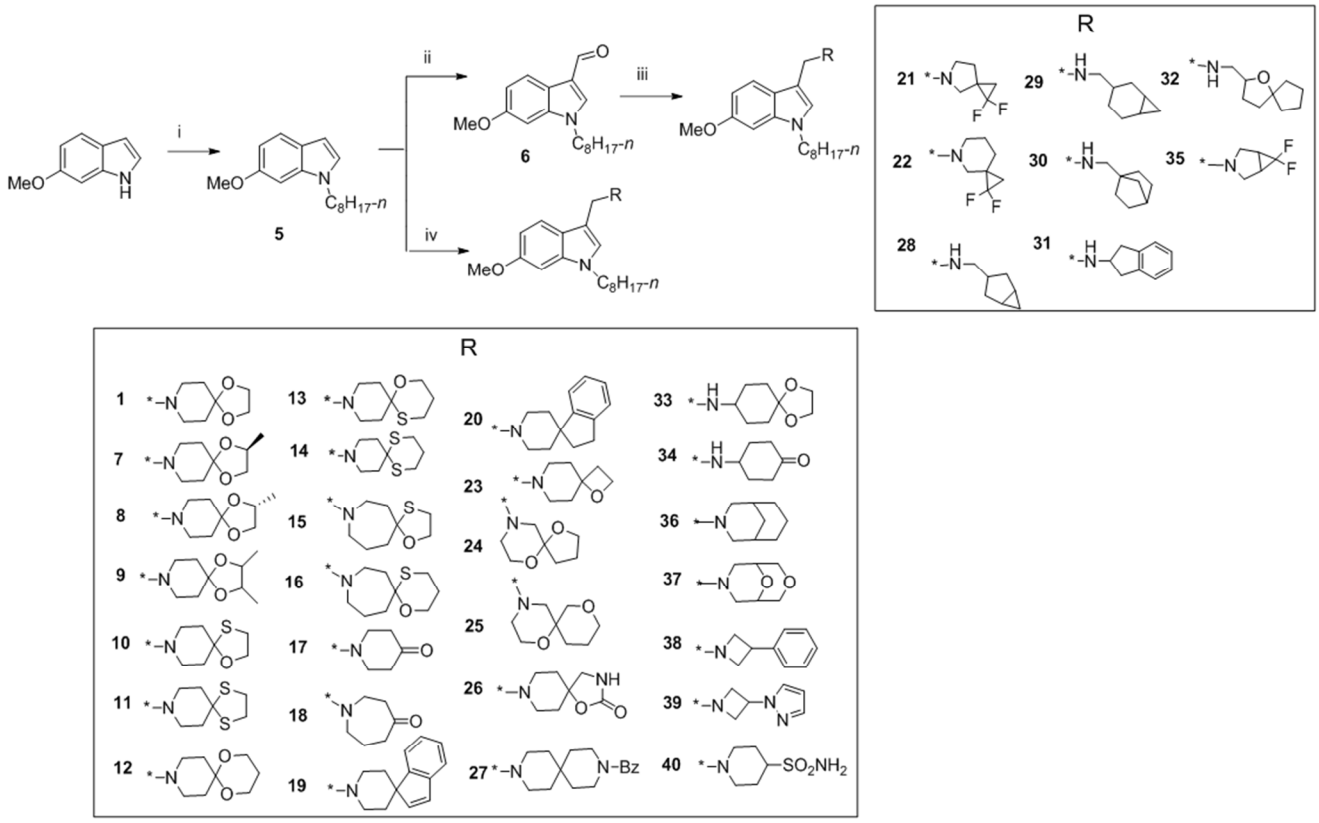

Scheme 1: Reagents and conditions: (i) NaH, $CH_3(CH_2)_6CH_2Br$, anhydrous DMF, 0 °C to RT, 2 – 8 h (ii) $POCl_3$, DMF, 0 °C – 40 °C, 2 h (iii) CH_3COOH, appropriate amines, $Na(AcO)_3BH$, anhydrous THF, RT, 24 – 48 h (iv) CH_2O (aq., 36%), appropriate amines, CH_3COOH, RT or $ZnCl_2$, EtOH, RT, 3 – 24 h.

Most of the amines indicated in Scheme 1 were commercially available but those required for **1, 7-16** were synthesized. These were the azaspirocycles 1,4-dioxa-8-azaspiro[4.5]decane (**1a**), (*S*)-2-methyl-1,4-dioxa-8-azaspiro[4.5]decane (**7a**), (*R*)-2-methyl-1,4-dioxa-8-azaspiro[4.5]-decane (**8a**), 2,3-dimethyl-1,4-dioxa-8-azaspiro[4.5]decane (**9a**), 1-oxa-4-thia-8-azaspiro-

[4.5]decane (**10a**), 1,4-dithia-8-azaspiro[4.5]decane (**11a**), 1,5-dioxa-9-azaspiro[5.5]undecane (**12a**), 1-oxa-5-thia-9-azaspiro[5.5]undecane (**13a**), 1,5-dithia-9-azaspiro[5.5]undecane (**14a**), 1-oxa-4-thia-8-azaspiro[4.6]undecane (**15a**) and 1-oxa-5-thia-9-azaspiro[5.6]dodecane (**16a**). These amines were prepared by reacting piperidin-4-one or azepan-4-one with the relevant alkanediols, alkanedithiols or mercaptoalkanols in the presence of catalytic amounts of *p*-toluenesulfonic acid.

In Series 2, we replaced the *n*-octyl side chain of **1, 12** and 6-methoxy-1-octyl-3-(piperidin-1-ylmethyl)-1*H*-indole (**52**) with various ring-bearing side chains, namely 3-phenoxypropyl, fluoro/methoxy/methyl-substituted 3-phenoxypropyl, 4-phenoxybutyl, 3-benzyloxypropyl, cinnamyl, 3-phenylpropyl and 4-phenylbutyl. Of these side chains, phenoxypropyl bromide (**53**) and 1-(3-bromopropoxy)-4-methoxybenzene (**54**) were prepared by reacting phenol / 4-methoxyphenol with 1,3-dibromopropane in the presence of potassium carbonate in acetonitrile (Supporting Information, Scheme S1). Scheme 2 outlines the synthesis of Series 2 which involved firstly, *N*-alkylation of 6-methoxy-1*H*-indole as described in Scheme 1 to give the 1-ring substituted 6-methoxyindoles (**41-51**), followed by the Mannich reaction with bases **1a, 12a** and piperidine to give the desired compounds (**41a,b,c – 50a,b,c; 51a,b**). The 1-octylindolyl Mannich base **52** was synthesized by a similar method. [10]

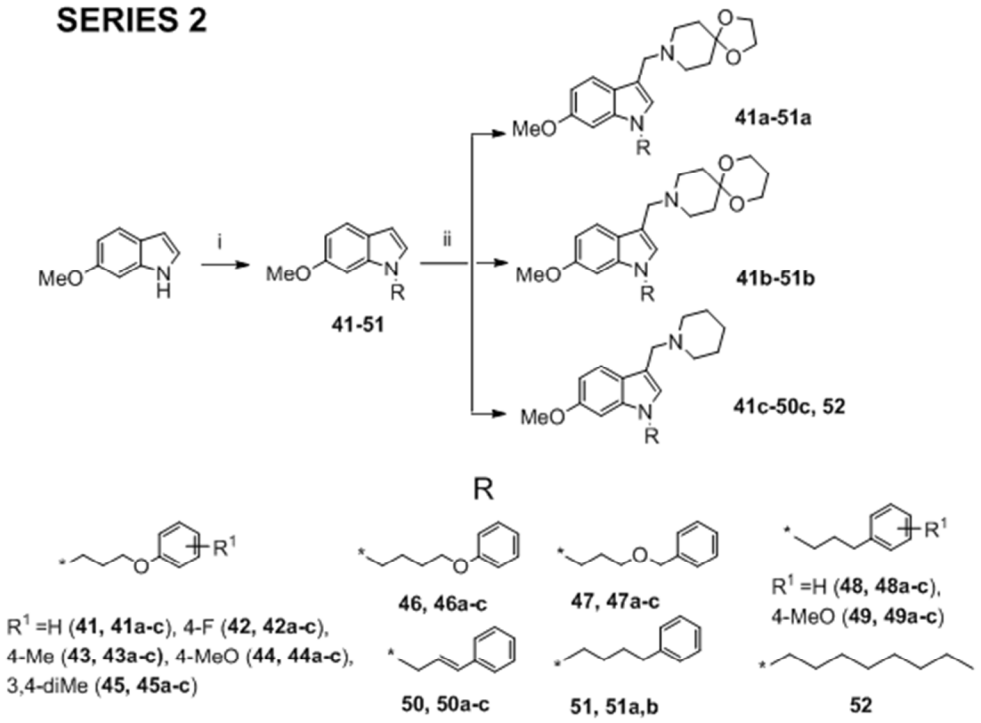

Scheme 2: Reagents and conditions: (i) NaH, appropriate *n*-octyl, phenalkyl, phenoxyalkyl, benzyloxyalkyl or cinnamyl bromide, anhydrous DMF, 0 °C to RT, 2 – 8 h (ii) CH_2O (aq., 36%), amines (**1a, 12a** or piperidine), CH_3COOH, RT or $ZnCl_2$, EtOH, RT, 3 – 24 h.

In Series 3, other functionalities (nitro, cyano, propoxy, isopropoxy, benzyloxy) were introduced in place of methoxy on the indole ring while retaining *n*-octyl and selected Mannich bases at positions 1 and 3 respectively. The 6-isopropoxy (**55a**), 6-propoxy (**55b**) and 6-benzyoxyindoles (**55c**) were synthesized from 6-hydroxy-1*H*-indole and the corresponding alkyl/benzyl halide in the presence of an inorganic base (cesium carbonate Cs_2CO_3 or potassium carbonate K_2CO_3) in DMF. The regioisomeric nitroindoles and 6-cyanoindoles were purchased. The substituted indoles were then alkylated with 1-bromooctane and reacted via a Mannich reaction to give the final compounds **57a-h, 58a-e** and **59a-c** (Scheme 3).

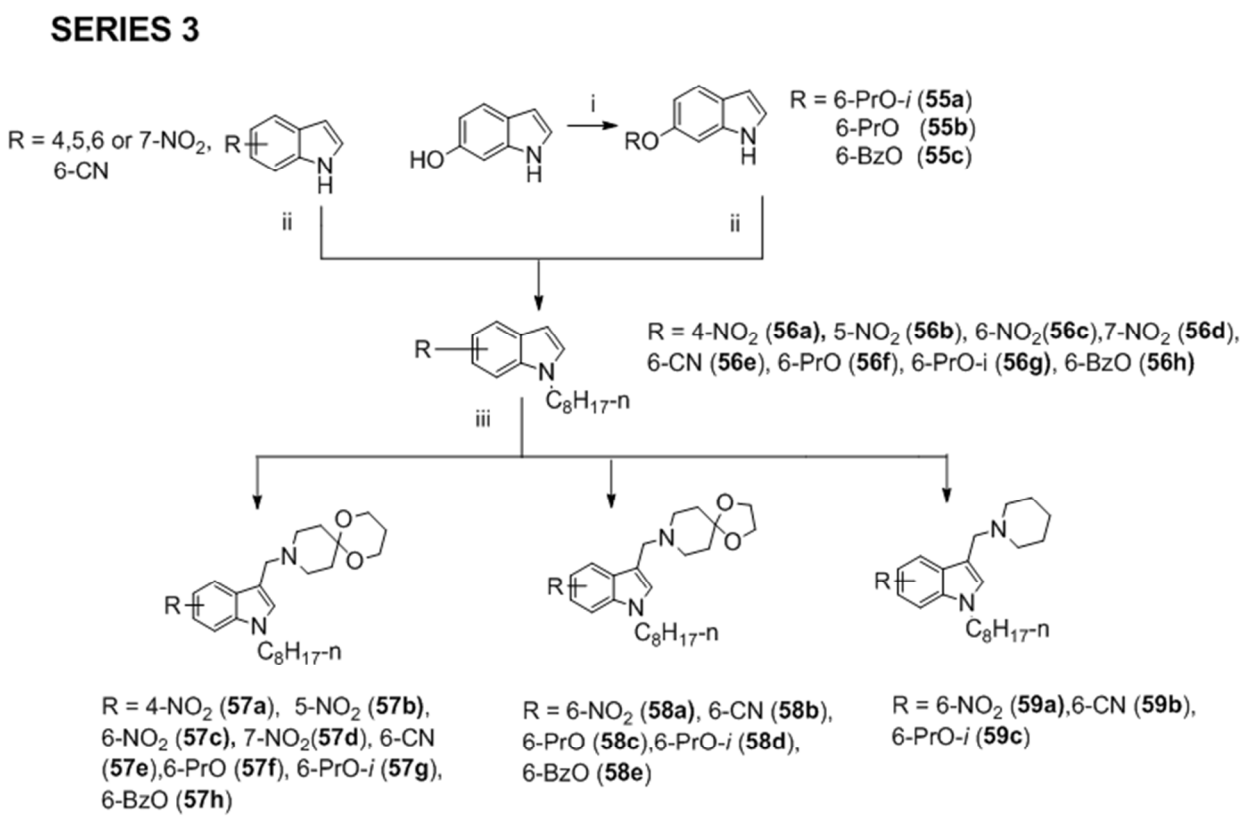

Scheme 3: Reagents and conditions: (i) 1-iodopropane; 2-iodopropane; or benzyl bromide, K_2CO_3 or Cs_2CO_3, anhydrous DMF, 80 ºC, 3 – 4 h (ii) NaH, $CH_3(CH_2)_6CH_2Br$, anhydrous DMF, 0 °C to RT, 2 – 8 h (iii) CH_2O (aq., 36%), amines (**1a, 12a** or piperidine), CH_3COOH, RT or $ZnCl_2$, EtOH, RT, 3 – 24 h.

To obtain Series 4, we first reacted regioisomeric 4-, 5-, 6- and 7-hydroxy-1*H*-indoles with 1-bromo-3-chloropropane or 1-bromo-2-chloroethane in the presence of K_2CO_3 in ethanol to obtain the chloropropoxyindole (**60a-d**) or 5-(2-chloroethoxy)-1*H*-indole (**60e**). Displacement of the terminal chlorine with iodine followed by reaction with amines azepane, 1,5-dioxa-9-azaspiro [5.5]undecane (**12a**), piperidine, (*S*)-2-methyl-1,4-dioxa-8-azaspiro[4.5]decane (**7a**), and pyrrolidine in the presence of K_2CO_3 or direct reaction of **60a-e** with the appropriate amine and Cs_2CO_3 gave **61a-b, 62a-c, 63, 64a-d, 65a-e**. The latter were then alkylated as before to give **66a-b, 67a-c, 68, 69a-d, 70a-e**.

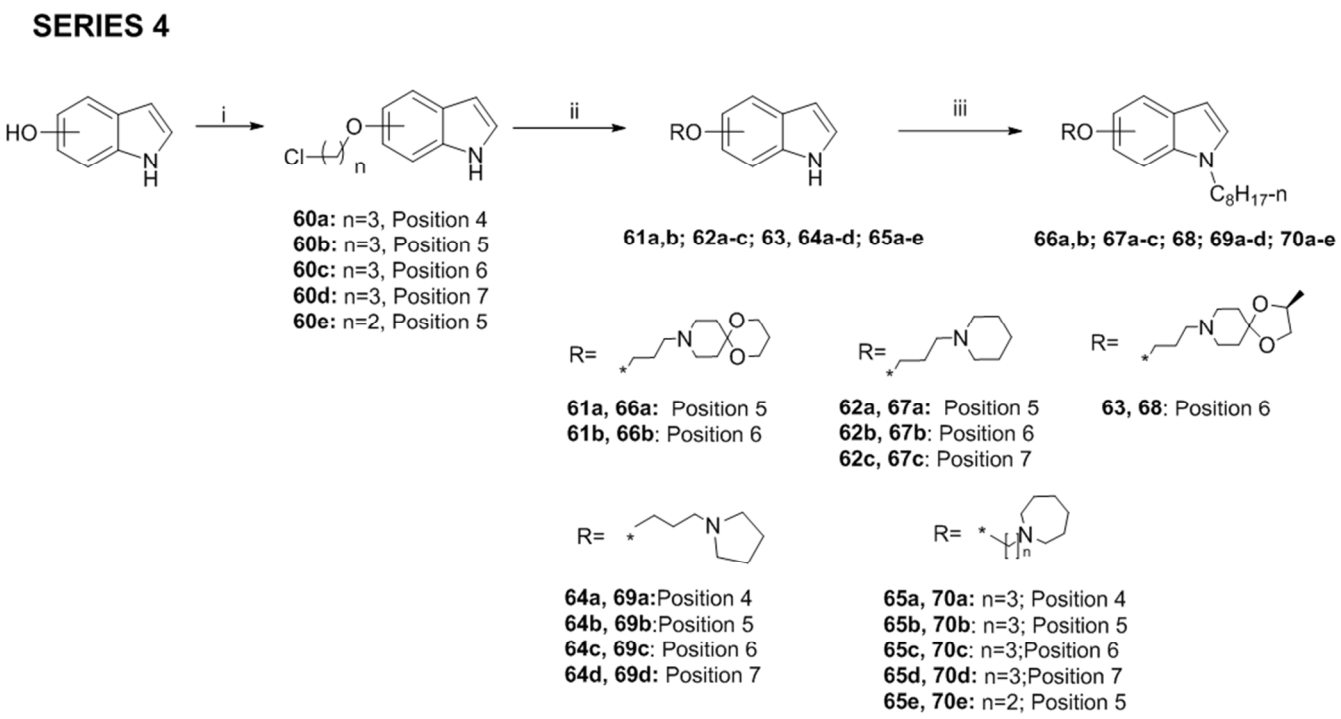

Scheme 4: Reagents and conditions: (i) 1-Bromo-3-chloropropane or 1-bromo-2-chloroethane, K_2CO_3, ethanol, reflux, 3 h (ii) KI, K_2CO_3, appropriate amine, MeCN, reflux, 24 – 48 h; or Cs_2CO_3, appropriate amine, MeCN, reflux, 24 – 48 h (iii) NaH, $CH_3(CH_2)_6CH_2Br$, anhydrous DMF, RT, 12 – 24 h.

RESULTS AND DISCUSSION

Series 1 compounds with azaspiroketal and isosterically related sidechains have submicromolar potencies and outstanding selectivity

The minimum inhibitory concentrations (MIC_{50}, MIC_{90}) of Series 1 were determined by turbidity measurements on *M. bovis* BCG, an attenuated tubercule bacillus and mycobacterial model organism (Table 1). The more potent analogs (MIC_{50} < 5 μM) were assessed on mammalian African Green Monkey kidney epithelial Vero cells for selective cytotoxicities. Also assessed were the hemolytic potential of some analogs on human red blood cells (RBCs). This was in view of the cationic amphiphilic nature of these compounds which would predispose them to non-selective membrane disruptive effects.

Table 1: Antimycobacterial activity (*M. bovis* BCG), mammalian Vero cell cytotoxicity (IC_{50}) and hemolytic activity (HC_{50}, human RBC) of Series 1 compounds.

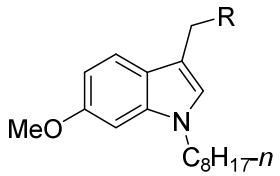

No	R	MIC (BCG) (μM)[a]		Vero IC_{50} (μM)[b]	SI[c]	HC_{50} (μM)[d]	LogP[e]
		MIC_{50}	MIC_{90}				
1	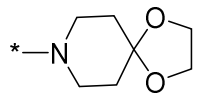	2	4	46	23	75	5.01
7	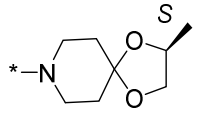	0.5	0.9	34	68	51	5.33
8	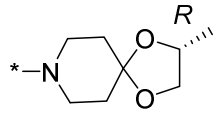	0.6	0.8	37	62	75	5.33
9	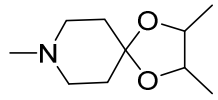	0.7	1.6	34	49	76	5.65
10	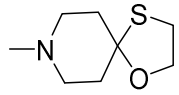	0.6	0.8	64	107	>300	5.73
11	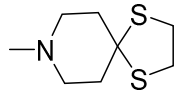	0.5	0.8	>200	>400	>300	6.46
12	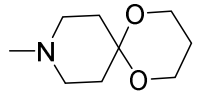	0.3	0.8	29	97	64	5.12
13	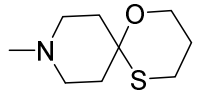	0.4	0.8	39	98	>300	5.84
14	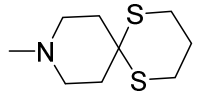	0.4	0.8	152	380	>300	6.56

15	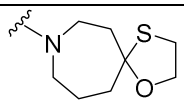	0.7	1.2	35	50	>300	5.70
16	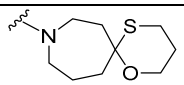	0.5	1	34	68	132	5.95
17	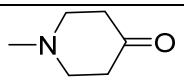	17	24	ND[f]	ND[f]	ND[f]	4.47
18	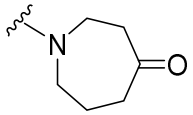	17	42	ND[f]	ND[f]	ND[f]	4.75
19	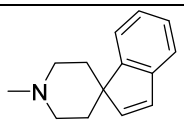	1	2	44	44	>300	6.93
20	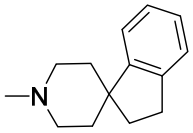	1	2	31	31	>300	7.25
21	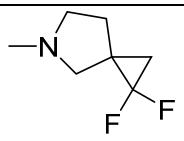	13	18	ND[f]	ND[f]	ND[f]	5.17
22	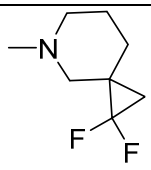	13	25	ND[f]	ND[f]	ND[f]	5.58
23	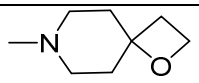	2	4	31	16	88	4.07
24	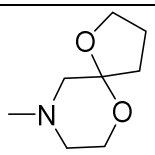	15	46	ND[f]	ND[f]	ND[f]	4.85
25	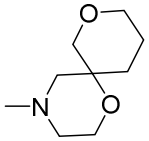	1.8	6.3	>500	>278	>300	4.16

26	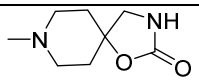	22	43	ND[f]	ND[f]	ND[f]	3.74
27	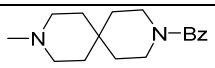	2.3	4.4	14	6	69	7.03
28	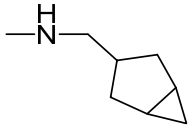	2	4	10	5	33	5.46
29	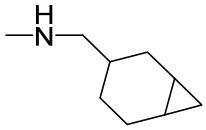	1.6	2.3	20	13	ND[f]	5.88
30	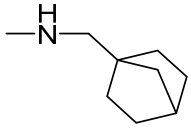	1.1	1.9	10	9	19	6.09
31	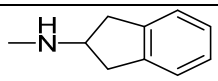	4	6	24	6	ND[f]	6.13
32	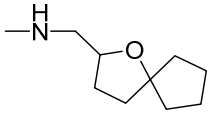	1.8	4.6	21	12	ND[f]	5.31
33	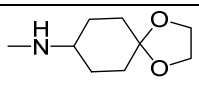	3.6	6.3	22	6	207	4.83
34	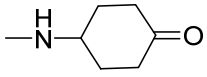	15	24	ND[f]	ND[f]	ND[f]	4.63
35	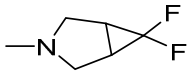	21	50	ND[f]	ND[f]	ND[f]	4.92
36	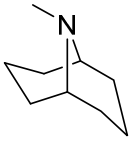	3.8	7.6	31	8	109	5.96
37	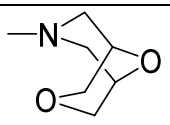	17	30	ND[f]	ND[f]	ND[f]	3.70

38	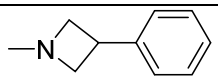	2	4	44	22	>300	6.07
39	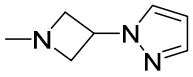	6	15	ND[f]	ND[f]	ND[f]	4.40
40	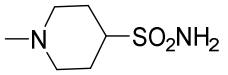	8	22	ND[f]	ND[f]	ND[f]	3.18

[a] Minimum Inhibitory Concentrations required to reduce growth by 50% (MIC_{50}) or 90% (MIC_{90}) compared to untreated controls. Average of 2 or more determinations. [b] Concentration required to reduce growth of Vero cells by 50% compared to untreated controls. Average of 2 or more determinations. [c] Selective Index = $IC_{50\ Vero}$ /$MIC_{50\ BCG.}$ [d] Concentration required to hemolyze 50% of human RBCs, compared to 2% Triton X-100 (100% hemolysis). [e] Log P values were determined on ChemDraw Professional Version 15.1.0.144. [f] ND = Not Determined

Structurally diverse Mannich bases were explored at R in Series 1 (Table 1). These were (i) azaspiroketals (**7-9**) and congeners in which one or both ketal oxygen atoms were replaced by sulfur (**10-16**); (ii) azaspirocycles without the ketal moiety (**19-27**); (iii) secondary amines substituted with fused/bridged bicyclic rings (**28-31**), the spirocycle 1-oxaspiro[4.4]nonane (**32**) and the spiroketal 1,4-dioxaspiro[4.5]decane (**33**); (iv) azabicycles (**35-37**) and (v) substituted azetidines **38,39** and piperidine **40**. Of these, only the azaspiroketals and their sulfur isosteres (**7-16,** MIC_{50} 0.3-0.7 μM) surpassed the original lead **1** (MIC_{50} 2 μM). These significant gains in potency which also led to better selective cytotoxicities, were achieved by modifying the ketal or piperidine ring of **1** in the following ways: (i) methyl or dimethyl substitution of the ketal ring; (ii) replacing one or both ketal oxygen atoms with isosteric sulfur to give **10** (MIC_{50} 0.6 μM) and **11** (MIC_{50} 0.5 μM); (iii) expanding the 5-membered ketal bearing ring to a 6-membered homolog (**12**, MIC_{50} 0.3 μM); (iv) submitting **12** to oxygen-sulfur isosteric substitution to give **13** and **14** (MIC_{50} 0.4 μM for both) and (v) homologation of the piperidine ring in **11** and **13** to the 7-membered azepanyl homologs **15** (MIC_{50} 0.7 μM) and **16** (MIC_{50} 0.5 μM) respectively.

Interestingly, these modifications resulted in compounds that were largely equipotent. We then asked if the narrow variation in MICs could be due to hydrolysis of the spirocyclic side chain to a common potent intermediate. Hydrolysis would yield the piperidinone **17** or azepanone **18** and if the hypothesis holds, these compounds should be as active as their spirocyclic precursors. That both **17** and **18** had only moderate activities (MIC_{50} 17 μM) led us to conclude otherwise.

The remaining compounds (**19-40**) in Series 1 were less potent than **1** but provided useful insight into the structural requirements for activity. First, the diminished activities of azaspirocycles that were not ketals (**19-27**) emphasized the importance of the intact azaspiroketal motif. Tellingly, the non-ketal azaspirocycles **24** and **25** displayed mediocre activity (MIC_{50} 15 μM, 1.8 μM), in spite of being regioisomers of the azaspiroketals **1** and **12** respectively. Second, positioning the basic nitrogen outside the spirocycle or bicycle resulted in analogs (**28-33**) that were moderately potent (MIC_{50} 1.1-4 μM) but with strikingly poor selective cytotoxicities (SI 5-13). The comparison of **1** (MIC_{50} 2 μM, SI =23) with **33** (MIC_{50} 3.6 μM, SI =6) was particularly compelling in this regard. As before, hydrolysis of the spiroketal side chain in **33** was dismissed in view of the limited activity of the *N*-cyclohexanone analog **34** (MIC_{50} 15 μM). Third, there was no apparent advantage in deploying rigid scaffolds like those in the azabicycles **35-37** or conformationally more flexible azacycles such as **38-40**.

We also collated the log P values of the Series 1 analogs. Lipophilicities varied over a wide 10^4 range, from 3.2 (**40**) to 7.3 (**20**) (Table 1). A cursory inspection showed that the least active compounds (MIC_{50} > 10 μM) had low log P values (3.2 – 5.6), an indication that activity may be driven by lipophilicity. Indeed, we found a significant inverse relationship beween MIC_{50} and log P (Spearman ρ correlation coefficient -0.567, p = 0.01, 2-tailed), althought the potent azaspiroketal Mannich bases (**7-16**), with an average log P of 5.8, were only moderately lipophilic.

In all, these results pointed to considerable tolerance for structurally diverse Mannich bases at R, most of which have low micromolar activities (MIC_{50} 1-10 μM). However, only azaspiroketals

and their sulfur isosteres (**7-16**) were uniquely associated with highly selective and submicromolar potencies.

Series 2 analogs with ring bearing side chains at the indole N were less potent than *n*-octyl counterparts.

Series 2 was designed to interrogate substitution at the indole N. Here, ring-bearing phenoxyalkyl, phenylalkyl and phenylalkenyl side chains were introduced in place of *n*-octyl. As shown in Table 2, the R^1 substitution was explored in three 6-methoxyindolyl Mannich bases, namely the early hit **1**, the potent submicromolar hit **12** and a previously reported piperidinylmethyl analog **52**. [10]

Table 2: Antimycobacterial activity (*M. bovis* BCG), mammalian Vero cell cytotoxicity (IC_{50}) and hemolytic activity (HC_{50}, human RBC) of Series 2 compounds.

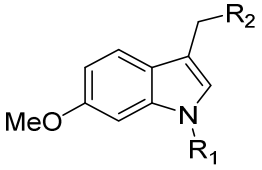

No	R^1	R^2	MIC (BCG) (μM)[a]		Vero IC_{50} [b]	HC_{50} (μM)[c]	LogP [d]
			MIC_{50}	MIC_{90}			
41a	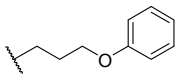	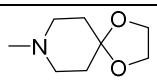	3	10	ND[e]	ND[e]	3.87
41b		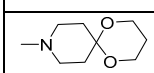	1.3	3.1	ND[e]	>300	3.98
41c		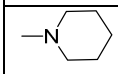	30	50	ND[e]	ND[e]	4.13
42a		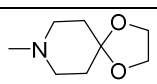	5	11	ND[e]	ND[e]	4.03

42b	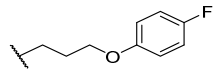	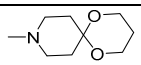	1.5	2.6	ND[e]	>300	4.14
42c		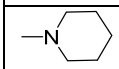	20	43	ND[e]	ND[e]	4.29
43a	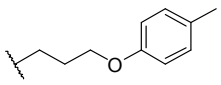	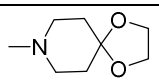	4.8	11	ND[e]	ND[e]	4.36
43b		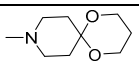	1.3	2.6	ND[e]	>300	4.46
43c		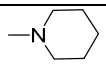	19	41	ND[e]	ND[e]	4.62
44a	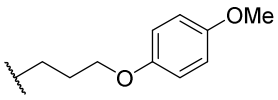	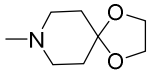	6	13	ND[e]	ND[e]	3.75
44b		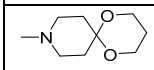	1.5	3.5	46	>300	3.85
44c		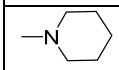	34	>50	ND[e]	ND[e]	4.00
45a	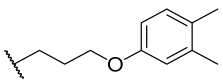	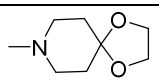	4.6	11	ND[e]	ND[e]	4.85
45b		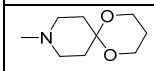	1.7	2.7	ND[e]	>300	4.95
45c		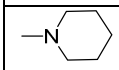	18	25	ND[e]	ND[e]	5.10
46a	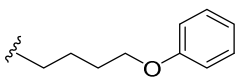	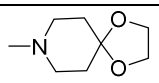	20	41	ND[e]	ND[e]	4.33
46b		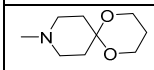	11	25	ND[e]	ND[e]	4.43
46c		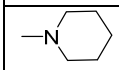	16	41	ND[e]	ND[e]	4.58
47a	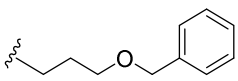	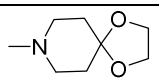	16	40	ND[e]	ND[e]	3.78
47b		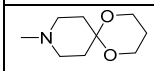	2.0	6	54	ND[e]	3.89
47c		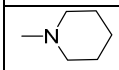	46	>50	ND[e]	ND[e]	4.04

48a	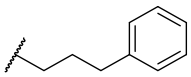	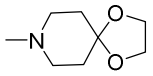	6	18	35	ND[e]	4.53
48b		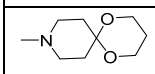	2.6	9.8	ND[e]	ND[e]	4.64
48c		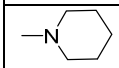	36	>50	43	ND[e]	4.79
49a	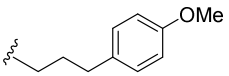	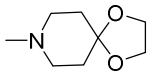	7.4	17	31	ND[e]	4.41
49b		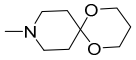	4.1	9.3	ND[e]	ND[e]	4.51
49c		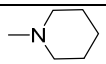	18	39	ND[e]	ND[e]	4.66
50a	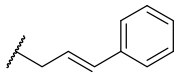	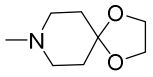	15	31	ND[e]	ND[e]	4.35
50b		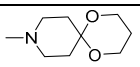	4.8	9	ND[e]	ND[e]	4.46
50c		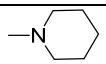	31	49	ND[e]	ND[e]	4.61
51a	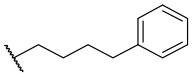	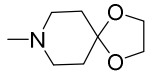	4.9	11.5	ND[e]	ND[e]	4.95
51b		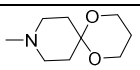	1.6	3.1	21	>300	5.05
1	- C_8H_{17-n}	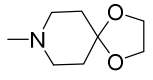	2	4	46	75	5.01
12		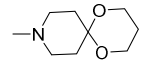	0.3	0.8	29	64	5.12
52		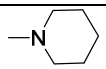	7	13	ND[e]	ND[e]	5.27

[a-d] As described in footnote of Table 1. [e] ND = Not Determined.

The results largely recapitulated the activity advantage of the R^1 *n*-octyl side chain that was observed in a related series where R^1 was varied from ethyl (-C_2H_5) to dodecyl (-$C_{12}H_{25}$) .[10] Here, none of the compounds with ring bearing R^1, for the same Mannich base R^2, were more potent than their *n*-octyl counterparts. Tellingly, the ring bearing analogs were also less lipophilic

than their n-octyl counterparts with the same R^2 group. However, unlike Series 1, Spearman correlation analysis did not reveal any significant relationship between MIC_{50} and log P in this series. However, it is still likely that the favored status of the *n*-octyl side chain is due to its lipophilic and less bulky features. As to whether there was an optimal ring bearing R^1, we found that this was largely determined by R^2. Of the three R^2 side chains explored, there was an unambiguous preference for the 6/6 spiro-ring fused 1,5-dioxa-9-azaspiro[5.5]undecane (**41b-51b**), followed by its 6/5 homolog 1,4-dioxa-8-azaspiro[4.5]decane (**41a-51a**) and lastly the monocyclic piperidine (**41c-50c**). For the 6/5 and 6/6 azaspiroketals, there was a preference for R^1 side chains that were phenoxypropyl (**41a,b**), substituted phenoxypropyl (**42a,b-45a,b**) and phenylbutyl (**51a,b).** Benzyloxypropyl at R^1 was favored only when paired with 1,5-dioxa-9-azaspiro[5.5]undecane at R^2 (**47b**).

The activity advantage of replacing 6-methoxy with other ring substituents in Series 3 was strongly dependent on the nature of the Mannich base

Series 3 was designed to explore the replacement of 6-methoxy with other groups while retaining the *n*-octyl chain and Mannich base (1,5-dioxa-9-azaspiro[5.5]undecanylmethyl, 1,4-dioxa-8-azaspiro[4.5]decanylmethyl, piperidinylmethyl) of Series 1 and 2 respectively (Table 3) . The electron donating methoxy was replaced by electron withdrawing groups (nitro, cyano) and sterically bulkier/ more lipophilic alkoxy groups (*n*-propoxy, isopropoxy, benzyloxy). To determine if there was a preference for specific positions on the indole ring, we prepared nitro regioisomers of the 1,5-dioxa-9-azaspiro[5.5]undecanyl analog **12** (Table 3). When greater potency was found for the 6-nitro regioisomer (**57c,** MIC_{50} 0.3 μM), subsequent substitutions were limited to position 6. Here, we found that 6-cyano (**57e**), 6-propoxy (**57f**), and 6-isopropoxy (**57g**) analogs were as potent (MIC_{50} 0.5-0.7 μM) as the 6-nitro **57c.** Only the insertion of the bulkier and more lipophilic benzyloxy at position 6 was not favored (**57h,** MIC_{50} 2.2 μM). Interestingly, none of the compounds were more potent than the 6-methoxy analog **12**.

In contrast, selective replacement of 6-methoxy in **1** and **52** resulted in more potent analogs. These were the 6-nitro **58a** (MIC_{50} 0.8 μM) and 6-cyano **59b (**MIC_{50} 2 μM) which were more potent than **1** and **52** respectively. Other substitutions yielded compounds (**58b-e, 59a,c)** that were comparable to **1** and **52**. Thus, R^3 substitution benefited the less potent analogs (**1, 52)** to a greater exent than the more potent **12**. Taken together, two structure-activity trends were evident: First, there was no preference for electron donating or withdrawing R^3 groups but size was a limiting factor. Notwithstanding, lipophilicity was not found to significantly influence activity. Second, the optimal R^3 in this series was conspicously influenced by the Mannich base at R^2, reinforcing the SAR trend observed in Series 2.

Table 3: Antimycobacterial activity (*M. bovis* BCG), mammalian Vero cell cytotoxicity (IC_{50}) and hemolytic activity (HC_{50}, human RBC) of Series 3 compounds.

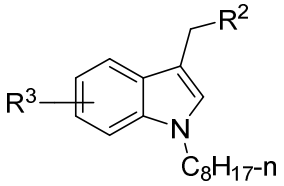

No	R^2	R^3	MIC (μM)[a]		Vero IC_{50} (μM)[b]	HC_{50} (μM)[c]	LogP [d]
			MIC_{50}	MIC_{90}			
57a	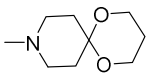	4-NO_2	10	25	ND[e]	ND[e]	5.13
57b		5-NO_2	7	18	ND[e]	ND[e]	4.92
57c		6-NO_2	0.3	0.8	28	>300	5.87
57d		7-NO_2	1.3	3.1	49	>300	6.06
57e		6-CN	0.5	1.2	22	>300	5.53
57f		6-$C_3H_{7\text{-n}}$	0.7	1.2	29	27	7.14
57g		6-$C_3H_{7\text{-i}}$	0.6	1.6	20	29	6.98

57h		6-BzO	2.2	3.1	27	>300	7.42
12		6-MeO	0.3	0.8	ND[e]	ND[e]	6.12
58a	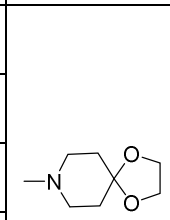	6-NO_2	0.8	1.6	62	>300	5.67
58b		6-CN	2.5	5	59	>300	5.33
58c		6-$C_3H_{7\text{-}n}$	3	5	29	31	6.94
58d		6-$C_3H_{7\text{-}i}$	3	6	41	56	6.78
58e		6-BzO	4	5.5	36	>300	7.21
1		6-MeO	2	4	ND[e]	ND[e]	5.92
59a	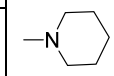	6-NO_2	4	5	23	ND[e]	6.35
59b		6-CN	2	6	22	ND[e]	6.01
59c		6-$C_3H_{7\text{-}i}$	4	6	26	ND[e]	7.46
52		6-MeO	7	13	ND[e]	ND[e]	6.60

[a-c] As described in footnote of Table 1. [d] Log P values were determined on ACD Labs Physchem History Version 12.5. [e] ND = Not Determined.

Non-Mannich base Series 4 analogs have modest antimycobacterial activities

The indole scaffold in Series 4 comprised an *n*-octyl side chain at position 1 and a basic spirocyclic or non-spirocyclic moiety attached to the benzenoid carbons of indole via an alkoxy linker. In a significant departure from the preceding series, these compounds retained the cationic amphiphilic signature but were not Mannich bases. Interestingly, this alteration resulted in analogs with mediocre activity (Table 4). Even analogs bearing the highly favored 6/6 spiro ring fused 1,5-dioxa-9-azaspiro[5.5]undecane ring (**66a, 66b**: MIC_{50} 6 μM, 14 μM), were no more potent than their non-spirocyclic piperidinyl counterparts (**67a-c**: MIC_{50} 5-13 uM). Clearly the privileged status of the azaspiroketal motif that was so pronounced in the indolyl Mannich bases of Series 1 did not apply to this scaffold. Here, the most potent members were **70b**

(MIC$_{50}$ 1.9 μM) and **70e (**MIC$_{50}$ 2 μM), both of which have azepanylalkoxy side chains. Collectively these results led us to conclude that the topography of the cationic amphiphilic indole was pivotal for activity. To this end, the location of the azaspiroketal moiety was decisive and reconfiguring it to a non-Mannich base was disadvantageous.

Table 4: MIC$_{50}$ / MIC$_{90}$ values of Series 4 on *M. bovis* BCG

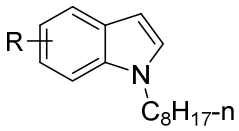

No	R	Position on ring	MIC (μM)[a]		LogP[b]
			MIC$_{50}$	MIC$_{90}$	
66a	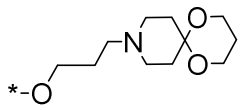	5	14	31	5.28
66b		6	5.6	28	5.28
67a	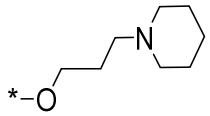	5	13	40	5.43
67b		6	13	25	5.43
67c		7	5	13	5.43
68	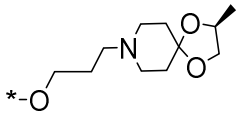	6	11	25	5.49
69a	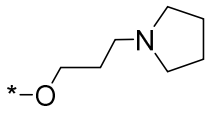	4	18	36	5.02
69b		5	31	48	5.02
69c		6	20	42	5.02
69d		7	10	22	5.02
70a	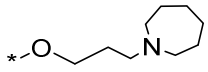	4	9.5	22	5.85
70b[c]		5	1.9	8	5.85
70c[d]		6	3.9	12	5.85
70d		7	5	11	5.85

70e	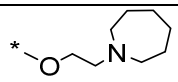	5	2	6	5.74

[a] As described in footnote of Table 1. [b] Log P values were determined on ChemDraw Professional Version 15.1.0.144. [c] Vero cell IC_{50} 34 μM. [d] Vero cell IC_{50} 33 μM.

Antimycobacterial profiles of azaspiroketals (10-14) with submicromolar potencies

Encouraged by the potent and selective antimycobacterial activities of the azaspiroketals **10-14**, we proceeded to investigate their antimycobacterial profiles in greater detail. As shown in Table 5, these compounds retained submicromolar MICs against pathogenic *Mtb* H37Rv. Both **12** and **13** were cidal against *Mtb* and achieved 1000-fold kill at 3.2 μM (4 x MIC_{90}). Together with remaining compounds**,** they were cidal against *M. bovis* BCG, with $MBC_{99.9}$ equivalent to 1-2x $MIC_{90\ BCG.}$ We also assessed the ability of **12** and **13** to eradicate non-growing, phenotyoically drug tolerant organisms by assessing their cidality on *Mtb* cultures grown under nutrient deprived conditions (Loebel model). Both compounds were cidal in this model, with LCC_{99} of 18 μM for **12** and $LCC_{99.9}$ < 18 μM for **13** (Supporting Information, Figure S1).

Table 5: Antimycobacterial profiles of Compounds **1, 10-14**

No	R [a]	*Mtb* H37Rv (μM)			*M.bovis* BCG (μM)	MIC_{50} (μM) (*M.bovis* BCG) in 7H9 Media [b]		
		MIC_{50} [b]	MIC_{90} [b]	$MBC_{99.9}$ [c]	$MBC_{99.9}$ [c]	Standard Medium [d]	Without Glycerol	With 10% FBS
1	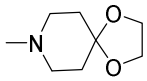	1.2	2.3	ND	3-6	1.5	1.6	1.1
10	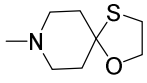	0.6	0.95	ND	0.8-1.6	0.36	0.37	0.32

11	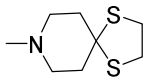	0.7	1.1	ND	0.8-1.6	0.29	0.27	0.28
12	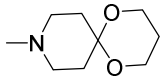	0.44	0.76	3.2	0.8-1.6	0.30	0.35	0.33
13	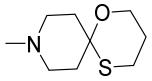	0.5	0.8	3.2	0.4-1.6	0.26	0.41	0.6
14	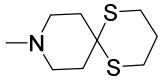	0.5	0.78	ND	0.8-1.6	0.28	0.43	0.48

[a] Refer to general structure given in Table 1; [b] Average of 2 or more separate determinations.

[c] $MBC_{99.9}$: Minimum bactericidal concentration required to kill 99.9% of bacteria. Average of 2 or more separate determinations. $MBC_{99.9}$ of **1, 10, 11, 14** on *Mtb* H37Rv were not determined (ND).

[d] Standard 7H9 medium contains glycerol and does not contain FBS

The antimycobacterial activities of **12, 13** and other analogs **(1, 10, 11)** were not dependent on media composition. MICs were unchanged in the absence of glycerol or in 7H9 medium containing serum. We also determined the spontaneous resistance mutation frequencies of *M. bovis* BCG and *Mtb* H37Rv to **12**. A low spontaneous mutation frequency (10^{-8}/CFU) was obtained on *Mtb* H37Rv exposed to **12** at 4 x and 8 x MIC_{90}. The *Mtb* H37Rv mutants were confirmed to be resistant to **12,** displaying on average 10-fold shifts in MIC_{50} values (based on analysis of 6 resistant strains). This is in contrast to the indolyl Mannich base 3-(azepan-1-ylmethyl)-4-fluoro-1-octyl-1*H* indole, **71** (Supporting Information, Figure S2) which we had reported earlier. [10] For compound **71** which was not an azaspiroketal Mannich base, the mutation frequency was < 10^{-9}/CFU for *M. bovis* BCG. [10] Here, we confirmed in side-by-side experiments that the spontaneous resistance mutation frequency of **71** was < 10^{-9}/CFU for *Mtb* H37Rv as well.

The azaspiroketal Mannich bases 10-13 disrupted the melting profiles of dimyristoylphosphatidylglycerol (DMPG) liposomal vesicles

Phosphatidylglycerols are negatively charged phospholipids that are abundant in bacterial plasma membranes but almost absent from membranes derived from eukaryotic cells. [20,21] Previously, we employed DMPG liposomal vesicles as surrogates of bacterial membranes and found that indolyl Mannich bases which altered the melting profiles of DMPG vesicles (monitored by differential scanning calorimetry) also permeabilized mycobacterial membranes as seen from greater propidium iodide (PI) uptake by mycobacterial cultures.[10] Conversely, antimycobacterial indolylalkyltriphenylphosphonium analogs that did not disrupt the thermotropic profiles of DMPG vesicles failed to increase PI uptake into mycobacteria. [11]

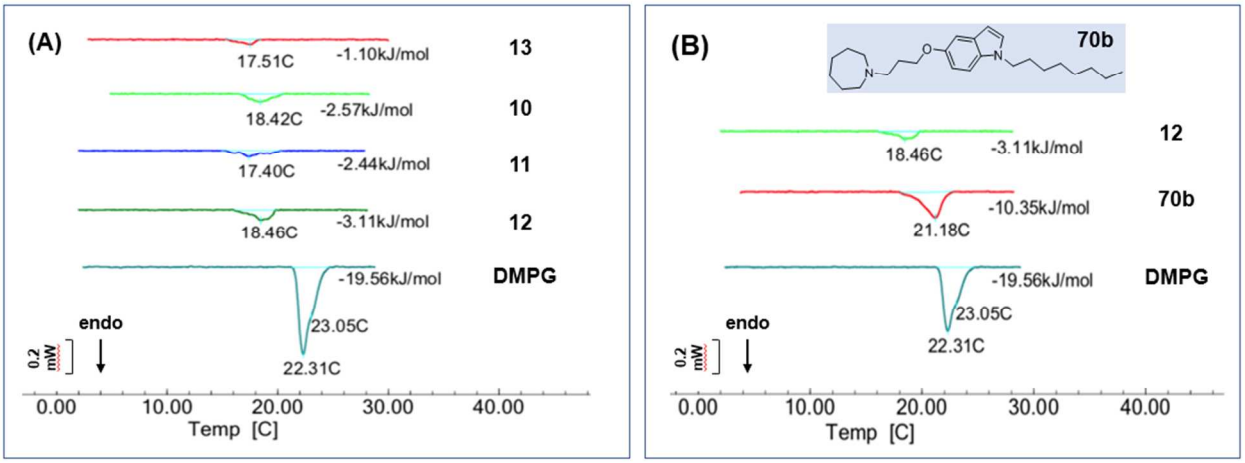

Figure 2: Representative calorimetric curves, in heating mode, of DMPG vesicles in the absence and presence (1 in 10 parts DMPG) of test compounds (A) **10-13**, and (B) **70b**. The melting transition Tm (^{o}C) and molar enthalpy ΔH (in kJ/mol) for each treatment condition are indicated. Control DMPG vesicles showed a main Tm (22.3^{o}C) and a shoulder at 23.05 ^{o}C. This appearance has been noted by others. [22]

Here, we found that **10-13** caused pronounced changes in the melting profile of DMPG vesicles (Figure 2). Their presence caused a downward shift ($\approx 4^{o}$) in the phase transition temperature Tm of the phospholipid and a pronounced 6-9 fold reduction in the calorimetric enthalpy (ΔH) of the gel to liquid transition. Collectively these changes pointed to weakened interactions within the lipid bilayer, conceivably due to the insertion of these compounds within the hydrophobic core of the bilayer. They also closely mimicked those reported earlier for DMPG vesicles containing **1**, determined under similar conditions. [10]

Intriguingly, the non-Mannich base **70b** of Series 4 had significantly diminished effects on the melting profile of the DMPG vesicles, namely a minimal (1^{o}) shift in Tm and a reduction of ΔH by only half (Figure 2B). Clearly, **70b** did not disrupt the DMPG vesicles to the same extent as **12**. It would seem that relocating the azaspiroketal in **70b** so that it is no longer part of a Mannich base had seriously hampered its interaction with the lipid bilayer.

The azaspiroketal Mannich bases 12 and 13 induced permeabilization of mycobacteria before onset of cell death.

In view of the perturbative effects of **10-13** on DMPG vesicles, we posited that they should permeabilize mycobacterial cells. Hence, changes in the permeability of *M. bovis* BCG cultures treated with representative members **12** and **13** (4x MIC_{90}) were monitored over time (up to 48h) using the nucleic acid dyes SYTO 9 and propidium iodide (PI). Similar experiments were carried out with the less potent analog **1** and isoniazid. Briefly, SYTO 9 is taken up by all cells and emits a green fluorescence whereas PI is selectively concentrated in cells with compromised membranes where it emits a red fluorescence. A decrease in the green/red ratio with time would signify progessive permeabilization of the mycobacterial cultures. The ratios were normalized against values obtained from untreated cultures (no permeabilization) and SDS-treated cultures (complete permeabilization) to give the % permeabilization. To confirm

that increased permeability was not an epiphenomenon of cell death, we monitored the viability of the treated cultures by plating and colony counting over the same time period.

Figure 3A shows the time-kill profiles of **12, 13** and isoniazid at 6 h, 12 h, 24 h and 48 h. The onset of cidal activity was more rapid for isoniazid but by 48 h, all three compounds had killed the mycobacterial cultures by more than 100-fold. The time-kill profile of **1** was determined separately and here we found that cultures treated with **1** were still viable at 48h (Figure 3B).

A comparison of the time kill profiles with the loss in membrane permeability at the various time points showed that **12** and **13** increased the permeability of bacteria before the onset of massive cell death. This was observed early for **13** (12 h) and later (24 h) for **12** (Figure 3C). **13** induced noticeably less permeabilization at 24 h than **12** but by 48 h, both compounds had permeabilized the cultures to the same extent. The slower acting **1** had a similar time-kill /permeability profile as **12,** except that permeabilization did not increase at 48 h (Figure 3D). These differences notwithstanding, the overall profile was one in which increased permeability was incurred early and *before* the onset of significant cell death, suggesting that increased permeability may have caused cell death. In the case of isoniazid, whose mode of action does not directly involve membrane disruption, both events – cell death and permeabilization – were aligned as would be expected if cell death was causal to the loss of the permeability barrier.

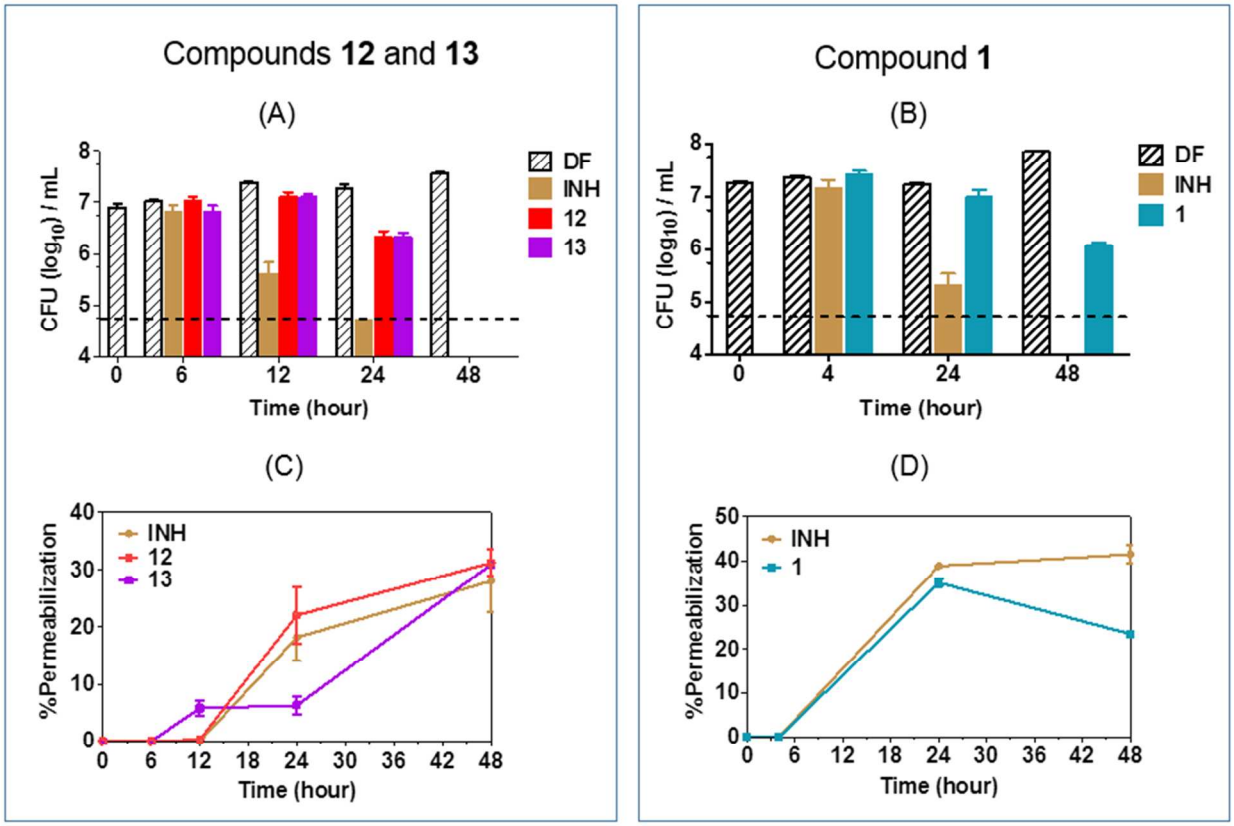

Figure 3: Time-kill kinetics (A,B) and membrane permeabilization (C,D) of *M. bovis* BCG cultures by test compounds (**1,12,13**) and isoniazid (INH). Mid log phase cultures were treated with (A) **12, 13** and (B) **1** over 48h at 4x MIC_{90} for the determination of time-kill profiles. Samples were concurrently withdrawn at the indicated time points for the determination of green/red fluorescence ratios, normalized to drug free (DF) inoculum at the same time point, to give % permeabilization induced by (C) **12, 13** and (D) **1.** Dashed lines in (A,B) represent the limit of detection. Experiments were performed 3 times independently. Mean and SD from representative experiments are shown

Compounds 12 and 13 induce the mycobacterial promoter p*iniBAC*

The promoter of the mycobacterial *iniBAC* operon is upregulated under conditions of cell envelope stress such as those encountered when cell wall biosynthesis is disrupted [23, 24] or when the mycobacterial membrane is permeabilized. [10] To further verify the membrane

disruptive effects of the azaspiro ketal Mannich bases, we monitored the fluorescent signal emitted by cultures of *M. bovis* BCG expressing Red Fluorescent Protein (RFP) under control of p*iniBAC* promoter, that had been treated with various concentrations (0.4 -100 μM) of **1, 12, 13** and the positive control isoniazid. Upregulation of transcriptional activity would increase the fluorescent signal of the RFP. Here we found that **12** and **13** increased the transcriptional activity of the p*iniBAC* in a concentration dependent manner (Figure 4). The p*iniBAC* activation profiles of **1, 12** and **13** were broadly similar to that of isoniazid. In all, the ability of **1, 12** and **13** to perturb phospholipid vesicles, permeabilize mycobacterial cultures and upregulate cell envelope stress reporter genes were in accord with their membrane disruptive properties.

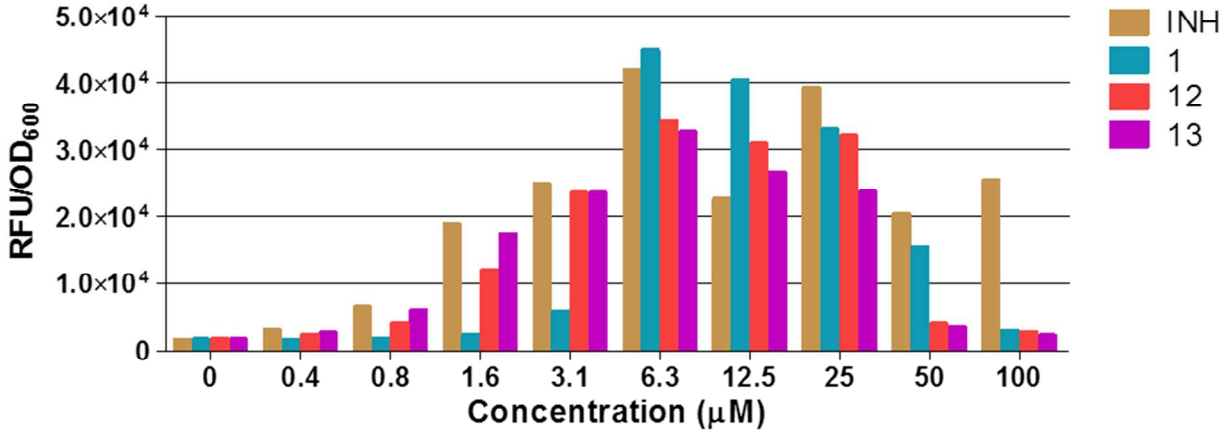

Figure 4: Concentration dependent induction of p*iniBAC* promoter activity by **1, 12, 13** and isoniazid (INH) in a recombinant strain of *M. bovis* BCG-p*iniBAC*-RFP after 24 h incubation. Experiments were performed in biological replicates, data shown here is from a representative experiment.

Compounds 12 and 13 did not depolarize mycobacterial membranes.

We expected the permeabilizing effects of the azaspiroketals on mycobacterial cultures to be accompanied by a loss in membrane potential. Hence, we examined the ability of **12** and **13** to dissipate the membrane potential of *M. bovis* BCG cultures over time (minutes to days) using the fluorescent membrane permeable dye 3,3-diethyloxacarbocyanine iodide ($DiOC_2$). Briefly, $DiOC_2$ emits red fluorescence in cells with polarized membranes and green fluorescence in cells that are depolarized. A fall in the red/green fluorescence ratio of $DiOC_2$ would indicate a loss in the membrane potential. Here, we monitored time dependent changes in the $DiOC_2$ ratios of *M. bovis* BCG cultures treated with **1, 12, 13**, the membrane depolarizer carbonyl cyanide m-chlorophenylhydrazine (CCCP) and rifampicin.

As shown in Figure 5, the changes in the $DiOC_2$ ratios of CCCP and rifampicin-treated mycobacteria reflected their roles as positive and negative controls respectively. In cultures treated with **12** and **13**, the $DiOC_2$ ratios were comparable to drug-free controls over the short time intervals (Figure 5A,B). Only at Days 3-5 did the ratios declined, by which time the losses would be attributed to the dying cultures. A similar observation was made for **1** (Supporting Information, Figure S3). Thus the azaspiroketal Mannich bases had the surprising effect of not depolarizing mycobacterial membranes in spite of their ability to induce permeabilization. There was however precedent to the separation of these closely related membrane effects. First, several antimycobactericidal indolylpentyltriphenylphosphonium analogs were found to rapidly depolarize *M. bovis* BCG cultures without inducing membrane permeabilization. [9] Second, Okano and coworkers reported that peripheral modifications of vancomycin resulted in a potent analog that increased permeability of *Enterococcus faecium* without inducing membrane depolarization or cell lysis.[25] The authors posited that the compound in question had a “specific” mode of action that could have led to membrane perturbation.

We had earlier reported that the indolyl Mannich base **71** (Supporting Iinformation, Figure S2) induced both permeabilization and depolarization of live *M. bovis* BCG cultures.[10] In view of the

present findings, we re-examined its effects on the membrane potential, specifically at shorter time intervals (minutes to hours) which were not investigated earlier. Here we found no depolarization at these early time points but were able to replicate the loss in membrane potential after 3 days (Supporting Information, Figure S4). Thus we concluded that the unusual uncoupling of permeabilization and depolarization of mycobacterial membranes was not unique to azaspiroketal Mannich bases (**1,12,13**) but a shared feature of non-azaspiroketal Mannich bases (as exemplified by **71**) as well.

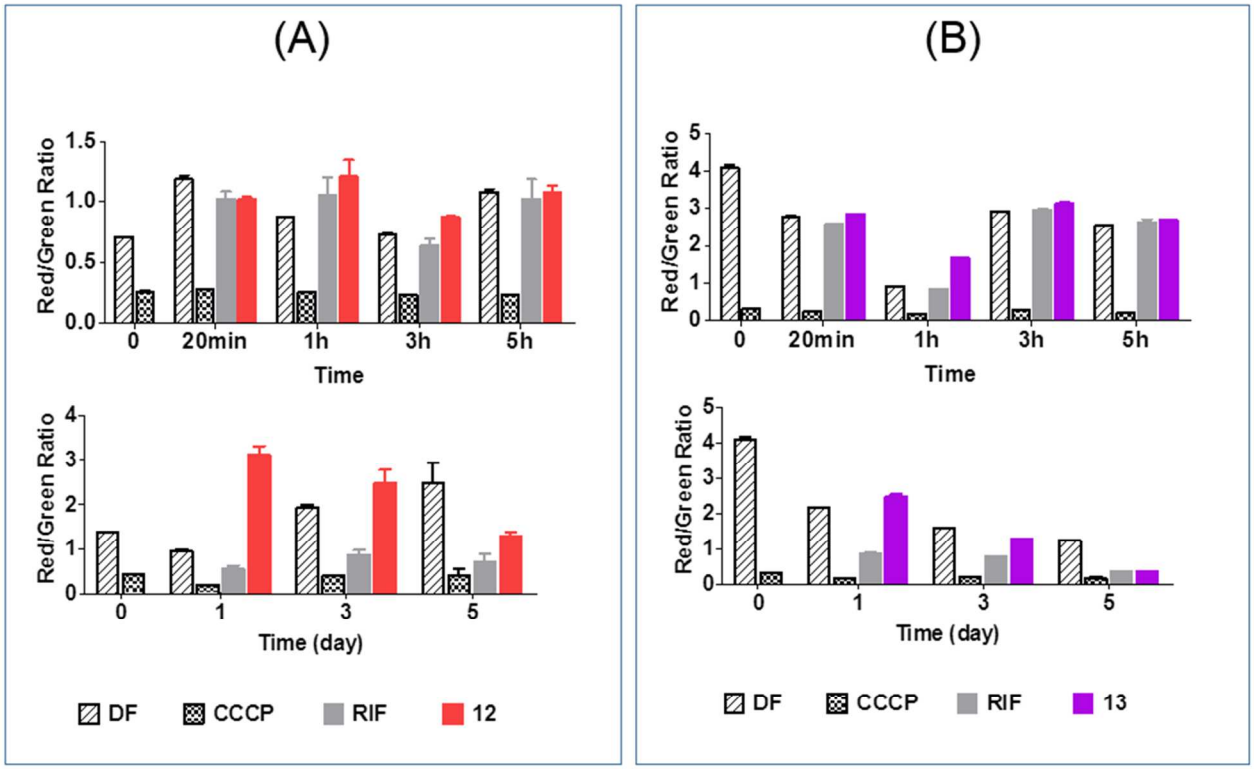

Figure 5: Changes in membrane potential (as reflected by Red/Green fluorescent ratio of $DiOC_2$ of *M. bovis* BCG cultures treated with (A) **12** and (B) **13** at 4x MIC_{90} over short time intervals (min – h, upper panel) and 1-5 days (lower panel). Rifampicin (RIF, 0.08 μM) and CCCP (100 μM) were negative and positive controls respectively. DF = Drug Free cultures. Results from 2-3 independent biological replicates.

Compounds 12 and 13 have limited electrophilic reactivity to cysteamine

3-Alkylindoles have been flagged out for their ability to generate electrophilic species. [26] Mechanistically, a similar reaction may occur with the indolyl Mannich bases. It would involve the displacement of the protonated basic nitrogen in the azaspirocyclic side chain of **12** or **13** to form a stabilized electrophilic carbocation that would react with soft nucleophiles (thiols, amines) in the biological milieu (Figure 6). This would implicate the scaffold as a pan-assay interference compound (PAIN) and hinder its progressability as an antimycobacterial pharmacophore.

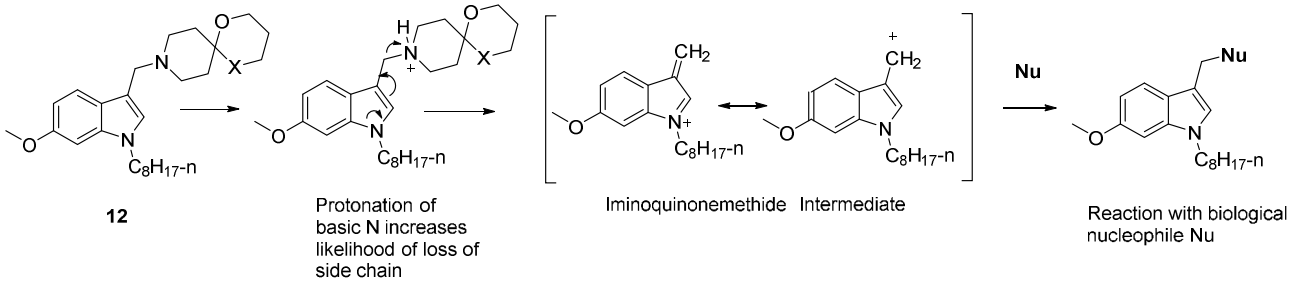

Figure 6: Proposed scheme by which **12** (X = O) or **13** (X = S) generates an electrophilic iminoquinonemethide intermediate. Nu = Nucleophile.

To address this possibility, the reactivity of **12** with the thiol reagent cysteamine was investigated by ^{1}H NMR. [27] Here we identified the signal assigned to the C-3 methylene protons of **12** and posited that a reaction with the thiol of the nucleophilic cysteamine would alter the chemical shift and appearance of this signal. The C-3 methylene protons of **12** were detected as a singlet at 3.67 ppm in deuterated DMSO- 1 % acetic acid. Downfield from this signal was a multiplet (3.77 ppm) attributed to the 6-methoxy protons and the spirocyclic methylene protons adjacent to the ketal oxygens (Figure 7A). Upon addition of cysteamine to the sample, the C-3 singlet shifted to 3.57 ppm but with no change in its appearance or the chemical shift of the flanking multiplet (Figure 7B). When the spectrum of the same sample was recorded at longer time intervals (30 min, 24 h), the C-3 methylene signal remained unaltered,

as were the signals assigned to adjacent multiplet (Figure 7C,D). The cysteamine methylene protons of cysteamine were detected at 2.6-2.8 ppm (multiplet) and remained unchanged over the monitoring period. Similar observations were made for **13** (Supporting Information, Figure S5). Thus, we surmised that the Mannich base side chains of **12** and **13** have limited electrophilic reactivity under the *in vitro* conditions of these experiments.

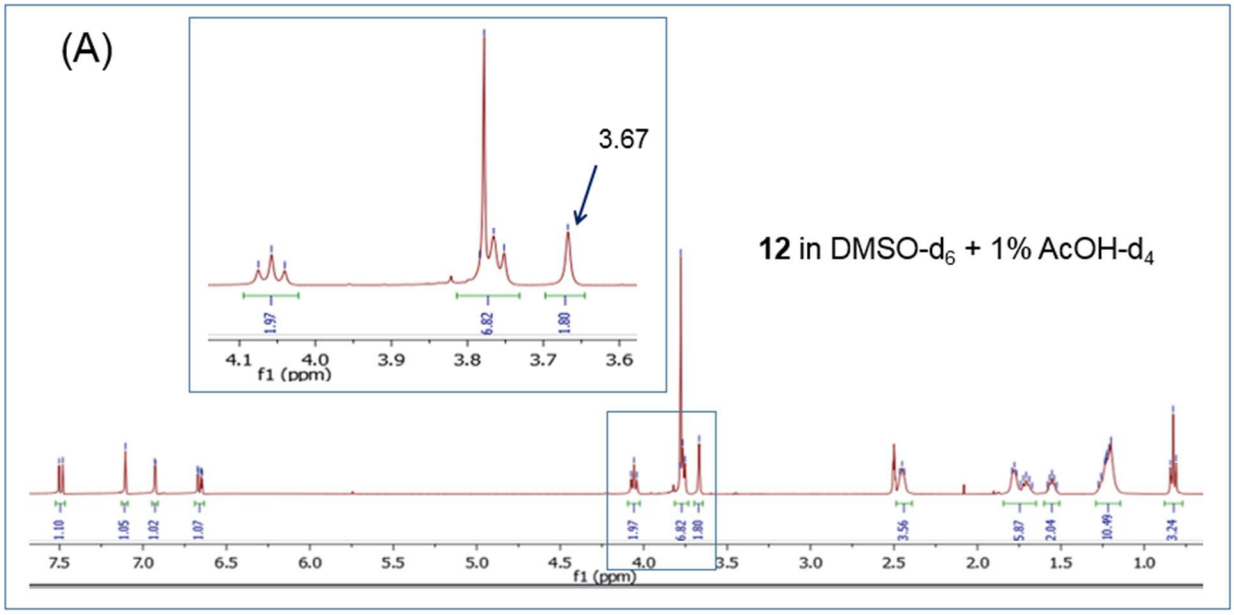

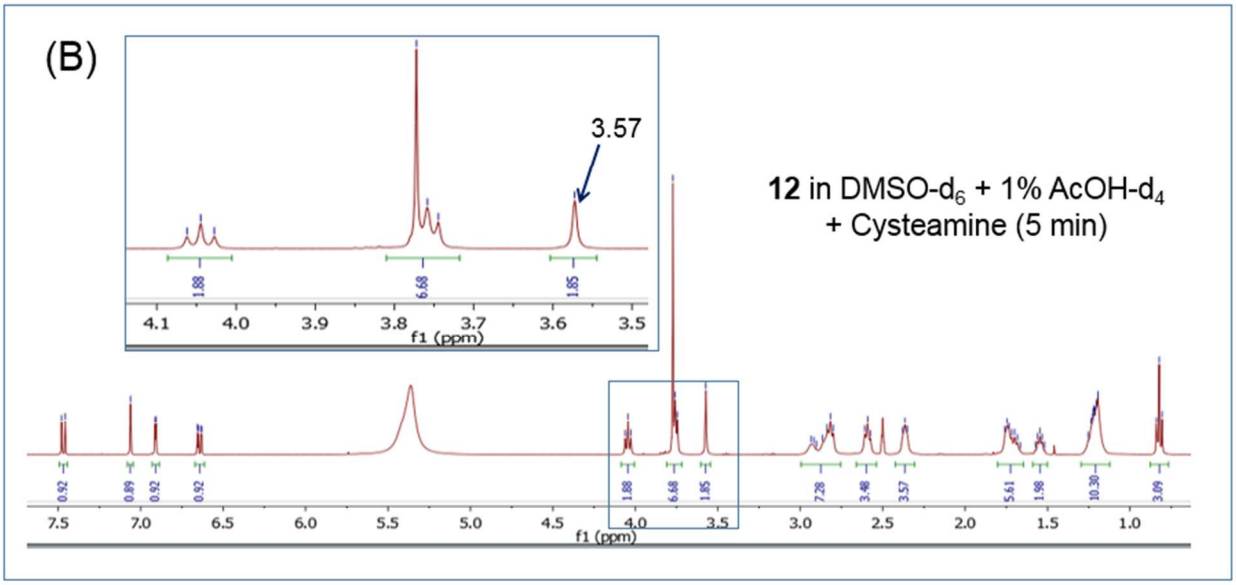

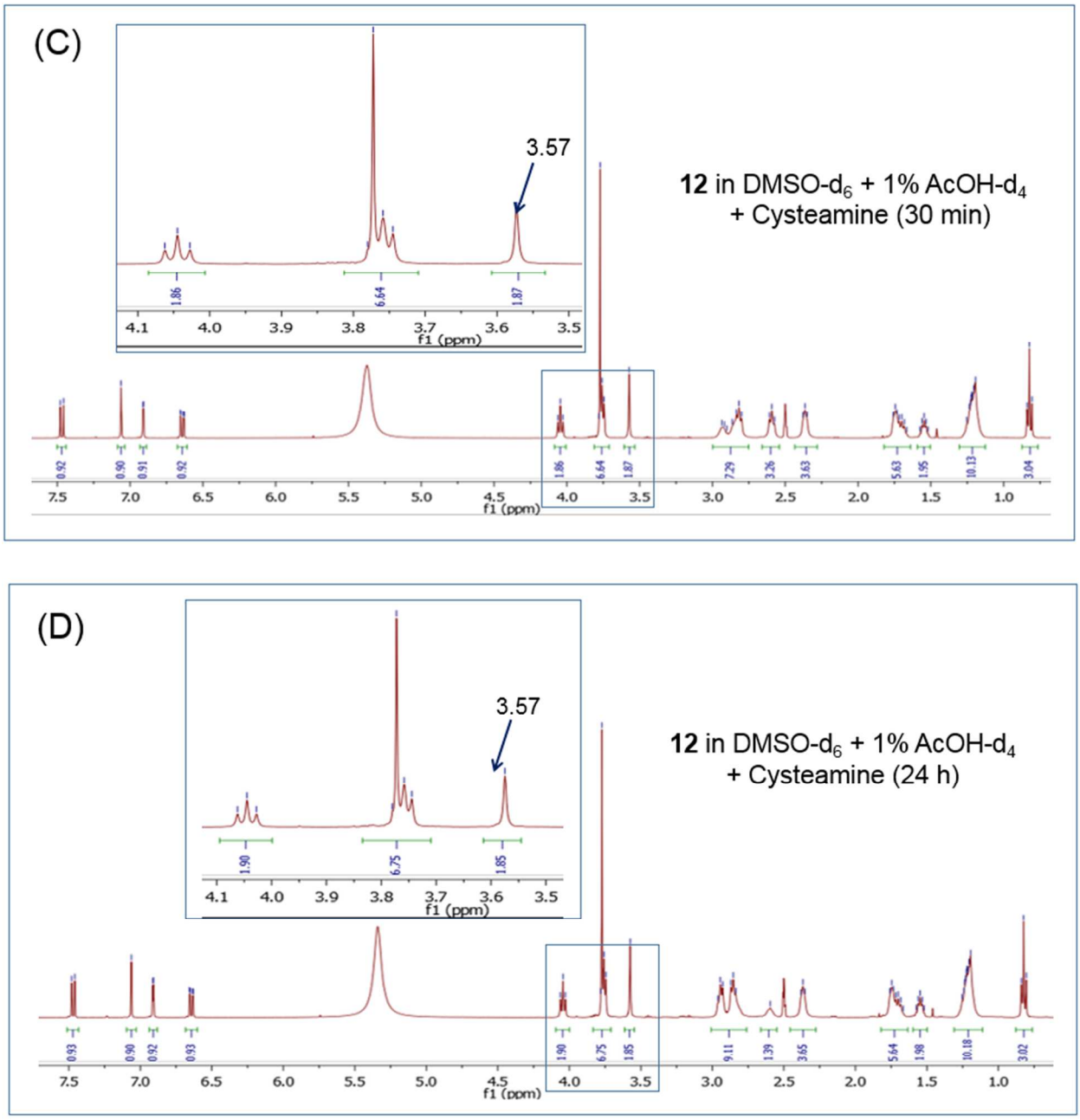

Figure 7: ^{1}H NMR spectra of **12** under different conditions: (A) In deuterated DMSO and 1% deuterated acetic acid with spectrum collected immediately (≈ 5 min); (B) As in (A) in the presence of cysteamine and spectrum recorded immediately (≈ 5 min); For (C) and (D), the spectra were recorded after 30 min and 24 h incubation with cysteamine respectively.

"Snapshot" PK of 12 and 13 in mice showed low plasma exposure but high lung partitioning

In view of their attractive mycobactericidal profiles, preliminary PK experiments were planned for **12** and **13**. Prior to these experiments, we assessed their PAMPA permeabilities, kinetic solubilities, and *in vitro* microsomal stabilities (Table 6). Concurrent experiments were carried out with **1.** No PAMPA Pe could be derived for **1, 12** and **13** due to their retention in the lecithin-dodecane lipid layer. In retrospect, this observation affirmed their affinities for lipid bilayers as reflected in the DSC experiments on model membranes. Their aqueous solubilities were largely similar (20-30 μM) but the longer half-lives of **12** and **13** suggested that they may be metabolically more stable to microsomal breakdown than **1.**

Table 6: Physicochemical profiles of **1, 12** and **13**

	1	**12**	**13**
Aqueous Solubility (μM) pH7.4 [a]	23.9 ± 0.8	27.5 ± 1.5	30.9 ± 1.3
PAMPA Effective Permeability (Pe) cm/s [b]	Cannot be determined	Cannot be determined	Cannot be determined
Half-Life (min), Rat male microsomes	17.4 ± 0.5	27.7 ± 0.6	32.9 ± 1.9

[a] Multiscreen filter plates (Millipore), 24 h agitation, 25°C, mean ± SD, n=3 determinations; [b] Multiscreen-IP PAMPA assay plates (Millipore), lecithin-dodecane as lipid layer, 24 h agitation, 25°C.

Next, we assessed the PK profiles of **1**, **12** and **13** in preliminary "snapshot" experiments carried out in CD1 mice. Briefly, two mice were dosed with the test compound at 25 mg/kg, administered orally in an aqueous solution of 5% dimethylacetamide-60% PEG300. This dose was well tolerated in the mice. Tail bleeds were collected from the treated animals at various time points (30min, 1h, 3h, 5h) and analyzed for their concentrations in plasma. Lung tissue was collected and analyzed at the terminal time point (5h). The analyses revealed that the compounds had low plasma exposures (33 ng/mL - 58 ng/mL) and high levels in lung tissue

(468 ng/g – 1596 ng/g) (Table 7). The preferential partitioning of these compounds in the lung may be due to their lipophilic character. However,additional time point determinations are required to confirm the selective lung distribution profiles of these compounds.

Table 7: Snapshot PK profiles of **1, 12** and **13** [a]

	1	**12**	**13**
Peak plasma concentration (ng/mL)	42.0	64.8	60.6
Area under the concentration time curve (AUC) (ng.h/mL)	173	282	224
Plasma concentration at 5 h (ng/mL)	33.0	58.5	55.2
Lung concentration at 5 h (ng/g)	467.5	1408	1596
Ratio of lung concentration to plasma concentration (Lung\Plasma) at 5 h	14.2	24.1	28.9

[a] **1, 12** and **13** were administered at 25 mg/kg (PO) to CD1 mice (n=2 for each compound).

Compound 12 demonstrated *in vivo* efficacy in an acute TB mouse model

Next, **1** and **12** were evaluated for *in vivo* efficacy in an acute TB mouse model. In this model, the compound was administered orally to mice infected with *Mtb* H37Rv at 100mg/kg daily over 4 weeks (6 days per week, total of 24 doses). Concurrent experiments were carried out with the positive control isoniazid at 25 mg/kg. Encouragingly, no adverse effects were detected in animals dosed with **1** or **12** throughout the treatment period, suggesting excellent *in vivo* tolerability of the compounds. At the end of this time, bacterial loads in the lungs and spleen were determined by plating organ homogenates on agar and subsequent colony counting (Figure 8). **12** significantly inhibited bacterial growth in both organs but **1** only reduced the splenic bacterial load. Although both **1** and **12** preferentially partitioned into lung tissue, we noted that the levels of **12** in lung (~3 μM) exceeded its *in vitro* $MIC_{90\ Mtb}$ (0.8 μM). In the case of

1, lung levels (~1 μM) and $MIC_{90\ Mtb}$ (2.3 μM) were nearly equivalent. Speculatively, this might have led to the different efficacy outcomes, although **12**, unlike isoniazid, was only bacteriostatic in this infection model.

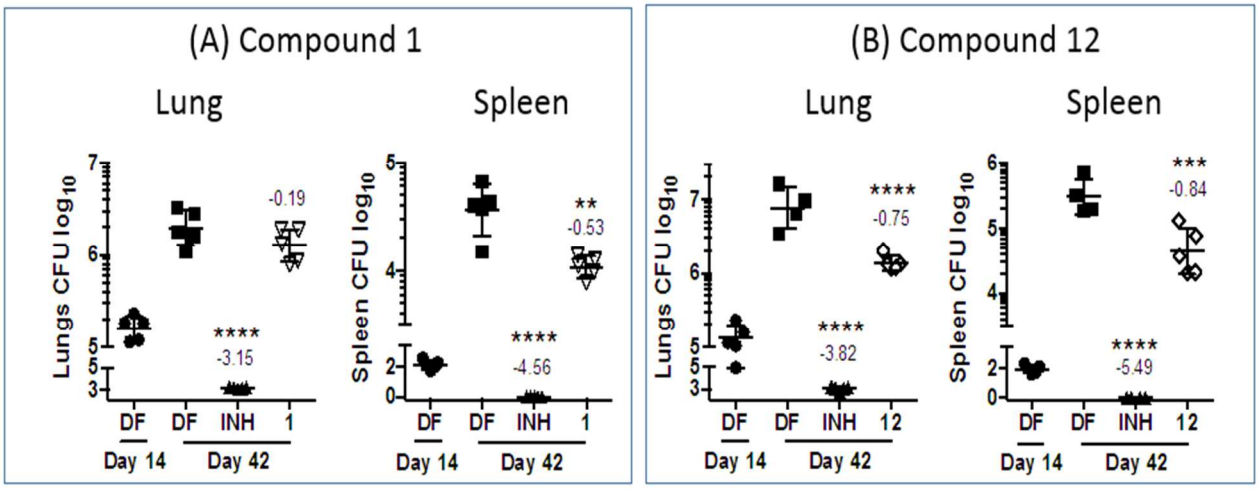

Figure 8: *In vivo* efficacy of (A) **1** and (B) **12** in a mouse model of acute TB. Mice were dosed with either drug at 100 mg/kg (po) for 6 days per week, x 4 weeks. A similar dosing schedule applied to isoniazid (INH) at 25 mg/kg. CFU analysis of lung and spleen tissues were carried out on treated mice and drug-free (DF) infected mice at Day 14 (start of treatment, Early Control) and Day 42 (end of treatment, Late Control). Statistical analysis was by One-way ANOVA, multi comparison, Bonferroni post test, n=4/5 (4/5 mice per group); $^{**}p<0.01$; $^{****}p<0.0001$. Figure depicts individual data points, means and SD. Numbers above groups reflect difference as compared to the drug free (DF) control at day 42 (Late Control).

CONCLUSIONS

The azaspiroketal is a uniquely rigid and three-dimensional motif that is occasionally found in antimycobacterial agents but whose contribution to activity has not been systematically explored. In this report, we have provided clarity on the potential of this motif as a potency

enhancing chemotype in a series of indolyl Mannich bases and affirmed the contribution of selective membrane perturbation to its mode of action.

The distinctive potency advantage of the azaspiroketal motif is predicated on the following evidence. First, it is supported by SAR garnered from Series 1-4. In Series 1, we showed that only specific changes to the 1,4-dioxa-8-azaspiro[4,5]decanyl side chain of the early hit **1** resulted in analogs with submicromolar MICs. These were methylation of the ketal ring, homologation of either ring in the spirocycle, and O to S isosteric replacement. The singularity of these requirements was emphasized by the failure of closely related modifications to achieve the same potency outcomes. Series 2 and 3 highlighted the azaspiroketal motif, notably 1,5-dioxa-9-azaspiro[5.5]undecanyl of **12**, as an influential driver of activity, prevailing over other modifications on the indole ring. From Series 4, we noted the striking losses in activity that followed when the azaspiroketal was not part of a Mannich base on the indole scaffold. Clearly it was not the azaspiroketal per se, but its inclusion in a Mannich base, that was pivotal to potency enhancement. The mechanistic implication of the latter remains an intrigue. The likelihood of the Mannich base as a source of reactive electrophilic species was explored but not found to be tenable. Second, the *in vivo* activity of **12** in an acute mouse model of TB validates the azaspiro ketal Mannich base as a potency enhancing chemotype. The apparent accumulation of **12** in lung tissue, as revealed in preliminary PK studies, may be a point in its favor. The *in vivo* studies also confirmed the low toxicity potential of the scaffold, as seen from **1** and **12** which were both well tolerated in mice.

The membrane disrupting effects of the indolyl azaspiro ketal Mannich bases were corroborated by their perturbative effects on model membranes, permeabilization of mycobacterial cultures and induction of the mycobacterial cell envelope stress reporter promoter p*iniBAC*. Our investigations on **12** and **13** provided further insight into this phenomenon. First, the membrane disruptive effects were specific to mycobacterial membranes. Both **12** and **13** induced minimal hemolysis of human red blood cells at their mycobactericidal concentrations. They were nearly

100-fold less cytotoxic against mammalian Vero cells and when administered *in vivo* to mice for PK studies, did not cause obvious adverse effects. Second, the cationic amphiphilicity of **12** and **13** is a necessary but not sufficient requirement for membrane disruption. This is convincingly demonstrated by the limited perturbation elicited by the Series 4 analog **70b** on DMPG vesicles. **70b** retains the cationic amphiphilic features of **12** but is not a Mannich base. The presence of the latter appears to be essential for membrane disruption. Third, **12** and **13** permeabilized mycobacterial membranes without dissipating the membrane potential. This profile is not uniquely associated with azaspiroketal Mannich bases but characteristic of indolyl Mannich bases, including those without the azaspiroketal side chain as seen with **71**. Lastly, whereas resistant mycobacteria could not be isolated for **71**, we were able to raise resistant mutants to **12** which was highly unusual as membrane disrupting agents typically have very low mutation resistance frequencies in view of their effects on multiple targets. Perhaps **12** intercepts a membrane target besides perturbing membranes and it is the interplay of these effects that have led to its exceptional mycobactericidal potency. Further investigations would be required to address this question.

EXPERIMENTAL

General chemistry

Reagents were of synthetic grade (or better) and were used without further purification. Reactions were monitored by TLC on aluminium-backed sheets coated with silica gel 60 (Merck) with visualization by UV. Compounds were purified by column chromatography on silica gel 60 (230-400 mesh, Merck). ^{1}H and ^{13}C NMR spectra were recorded at 400 MHz and 101 MHz respectively on a Bruker 400 Ultrashield Plus Instrument (Bruker, Billerica, MA, USA) in $CDCl_3$, DMSO-d_6, or MeOH-d_4 at room temperature. Chemical shifts were reported in parts per million (ppm) on the δ scale using residual protio-solvent signals (^{1}H NMR: $CDCl_3$ δ7.26, DMSO-d_6 δ2.50, MeOH-d_4 δ4.78; ^{13}C NMR: $CDCl_3$ δ77.00) as internal references. Coupling constants

(*J*) were reported in Hertz (Hz) and splitting patterns as singlet (s), broad singlet (s, br), doublet (d), triplet (t), quartet (q), quintet (quint), sextet (sext), septet (sept), doublet of doublets (dd), doublet of triplets (dt) or multiplet (m). Nominal mass spectra were captured on a LCMS 2020 LC/MS System (Shimadzu, Singapore) by ESI or dual ion source (ESI,APCI), run in either positive or negative ionization mode. High-resolution mass spectra were recorded on a Bruker micrOTOFQII mass spectrometer (Bruker, Billerica, MA, USA) by ESI (positive ionization mode). Purities of final compounds were determined by reverse-phase HPLC using Zorbax Eclipse XDB-C_{18} column (5 µM, 150 x 4.6 mm) and found to be > 95%. Spectral and other details of synthesized compounds are given in Supporting Information.

General procedure A for the synthesis of *N*-substituted indoles in Series 1(5), Series 2 (41-49, 51), Series 3 (56a-56h) and Series 4 (66a,b, 67a-c, 68, 69a-d, 70a-e).

A previously reported method was followed. [10] Briefly, the substituted indole (1 eq) was reacted with sodium hydride (NaH, 60 % dispersion in mineral oil; 2 eq.) in anhydrous DMF (20 – 30 mL) in an ice bath for 20 min. 1-Bromooctane, phenylalkyl bromide or phenoxyalkylbromide (2 eq) in DMF (5 mL) was added dropwise to the stirred mixture, after which stirring was continued at room temperature (RT) for 2-8h. Thereafter, isopropanol was added to quench the reaction, followed by methanol (dropwise) and then water. The crude product was extracted with dichloromethane (DCM, 3 x 20 mL), washed with water (2x) and brine (1x). The organic layers were combined, dried (anhydrous Na_2SO_4) and removed under reduced pressure to give the crude product which was purified by column chromatography using hexane: ethyl acetate (30: 1). Yields for target compounds ranged from 39 – 99 %.

1-Cinnamyl-6-methoxy-1*H*-indole (50)

A reported method was employed with modifications. [28] Briefly, ground potassium hydroxide (KOH; 336 mg, 6.0 mmol) was quickly weighed in a dry round-bottom flask and 10 mL acetonitrile (MeCN) was added with stirring at RT. Commercially available 6-methoxyindole (441 mg, 3.0 mmol) in 2 mL MeCN was added dropwise to the mixture, stirred for 15 min, followed by

addition of (*E*)-cinnamyl bromide (887 mg, 4.5 mmol). Stirring was continued for another 3 h, after which water (20 mL) and 1 M HCl (15 mL) were added in succession and the mixture extracted with ethyl acetate (EA, 3 x 15 mL). The combined organic layer was washed sequentially with water and brine, dried over anhydrous Na_2SO_4, filtered, and the solvent removed under reduced pressure to give the crude product which was purified by column chromatography (hexane: EA; 20: 1). **50** was obtained as a yellow oil in 57% yield. ^{1}H NMR (400 MHz, $CDCl_3$) δ 7.52 (dd, *J* = 2.4, 8.5 Hz, 1H), 7.39 – 7.27 (m, 5H), 7.05 (d, *J* = 3.1 Hz, 1H), 6.90 – 6.76 (m, 2H), 6.58 – 6.43 (m, 2H), 6.40 – 6.29 (m, 1H), 4.82 (ddd, *J* = 1.5, 5.7, 19.6 Hz, 2H), 3.86 (s, 3H); MS (ESI): Calculated for $C_{18}H_{17}NO$ 263.13, found 264.20 $[M+H]^+$.

General procedures (B, C) for the synthesis of the indolyl Mannich bases in Series 1 (1, 7-20, 23-27, 33, 34 36-40), Series 2 (41a,b,c – 50a,b,c; 51a,b) and Series 3 (57a-h, 58a-e, 59a-c).

Procedure B: To a stirred solution of the appropriate amine (1.2 eq.) in acetic acid (5 mL) was added the *N*-substituted indole (1 eq.) and formaldehyde (CH_2O; 36 % aqueous solution, 1.2 eq). [29] The reaction mixture was stirred at RT and monitored periodically by TLC. Upon completion of the reaction (3-24h), the mixture was made alkaline (pH 8) with NaOH (1M, 5-10 mL) and extracted with DCM (3x15 mL). The organic layer was washed with brine, dried (anhydrous Na_2SO_4) and concentrated under vacuum to give the crude residue which was purified by column chromatography using DCM: MeOH (gradient elution). Target compounds were obtained in yields ranging from 10 – 57 %.

Procedure C: The *N*-substituted indole (1 eq.) was added to a stirred solution or suspension of the amine, formaldehyde (36 % aqueous solution) and $ZnCl_2$ (1.2 eq. of each) in ethanol (3 – 5 mL) at RT. [30] The reaction was monitored by TLC and on completion (5-24h), the solvent was removed under reduced pressure and work up was carried out as described earlier. Target compounds were obtained in yields ranging from 10 – 75 %.

6-Methoxy-1-octyl-1*H*-indole-3-carbaldehyde (6)

A reported method was followed with modifications. [31] Briefly, a 50-mL round bottom flask was charged with DMF (15 mL) under an inert atmosphere (N_2) in an ice bath. Phosphorus oxychloride (6 mmol) was added dropwise over 30 min. Stirring was continued for 1.5h at 0 ºC during which time 6-methoxyindole (**5**, 4 mmol) in DMF (5 mL) was added dropwise. Stirring was continued at 40 ºC for 2 h, and then cooled to 0 ºC with crushed ice (50 g). The reaction mixture was adjusted to pH 8 with 1 M NaOH, extracted with DCM (3 x 20 mL) after which the organic layers were washed (brine), dried (anhydrous Na_2SO_4) and concentrated under reduced pressure to give the crude product which was purified by column chromatography (DCM, 100 %). **6** was obtained as a yellow solid (644 mg, 56% yield), mp 47 – 50 ºC. ^{1}H NMR (400 MHz, $CDCl_3$) δ 9.91 (s, 1H), 8.17 (d, *J* = 8.6 Hz, 1H), 7.59 (s, 1H), 6.95 (dd, *J* = 2.2, 8.6 Hz, 1H), 6.80 (d, *J* = 2.2 Hz, 1H), 4.08 (t, *J* = 7.1 Hz, 2H), 3.87 (s, 3H), 1.85 (quint, *J* = 7.1 Hz, 2H), 1.39 – 1.17 (m, 10H), 0.91 – 0.82 (m, 3H); MS (DUIS): Calculated for $C_{18}H_{25}NO_2$ 287.19, found 288.15 $[M+H]^+$.

General Procedure D for the synthesis of Series 1 compounds 21, 22, 28 – 32 and 35

The method by Abdel-Magid *et al.* was employed. [32] Briefly, to a solution of **6** (1 eq.) in tetrahydrofuran (THF, 5 mL) was added the amine (1.2 eq.) and acetic acid (2 eq.) dissolved in THF (2 mL). The reaction mixture was stirred for 30 min, sodium triacetoxyborohydride (3 eq.) was added, and stirring continued for 6 – 12 h or until complete as indicated by TLC (DCM: MeOH; 40: 1). A solution of 1 M NaOH (5 mL) was added to quench the reaction. After stirring for another 30 min, the reaction mixture was extracted with ethyl acetate (2 x 20 mL), washed with water (2 x 20 mL), brine, dried (anhydrous Na_2SO_4) and concentrated under reduced pressure to give the crude product which was purified by column chromatography (DCM: MeOH, gradient elution). The target compounds were obtained in yields ranging from 18 – 31 %.

General procedure E for the synthesis of azaspiro-fused intermediates (1a, 7a – 16a)

The method of Tiwari *et al* was followed with modifications. [33] Briefly, 2 eq of the diol (1,2-ethanediol, 1,3-propanediol, 2-mercaptoethanol, 3-mercapto-1-propanol, 1,2-ethanedithiol or 1,3-propanedithiol) and 4-piperidone monohydrate hydrochloride (1 eq) were dissolved in toluene (20 – 50 mL). *p*-Toluenesulfonic acid monohydrate (0.05-0.1 eq) was added and the reaction mixture heated to reflux. A Dean-Stark apparatus was attached to the reaction vessel to collect water released during the reaction. When no more water was collected, the mixture was cooled to RT, toluene was removed under reduced pressure and the crude product used as such for the subsequent Mannich reaction without further purification. 4-Azepanone HCl was reacted with 2-mercaptoethanol and 3-mercapto-1-propanol to give **15a** and **16a** respectively under similar conditions.

General procedures F for the synthesis of (3-chloropropoxy)indoles (60a-d) and 5-(2-chloroethoxy)indole (60e)

The method of Lepri *et al.* was followed with modifications. [34] Briefly, 1-bromo-3-chloropropane (3 eq.) was dissolved in ethanol (20 – 30 mL). K_2CO_3 (6 eq.) was added with stirring at RT, followed by an ethanolic solution of the commercially available 4-, 5-, 6-, or 7-hydroxyindole (1 eq., 5 mL). The reaction mixture was then refluxed at 80 ˚C for 3 – 5 h. The reaction was monitored by TLC (hexane: ethyl acetate, 2: 1) and cooled to RT on completion. Solvent was removed under reduced pressure and the crude residue extracted with DCM (3 x 20 mL). The organic layer was washed successively with water and brine, dried (anhydrous $MgSO_4$), concentrated under reduced pressure to give the crude product which was purified by column chromatography (hexane: ethyl acetate, 30: 1, or DCM 100 %) to give **60a-d** in yields ranging from 42 % to 71 %. 1-Bromo-2-chloroethane was reacted with 5-hydroxyindole in the same way to give **60e** in 20 % yield.

General procedure G for the synthesis of (3-amino)propoxyindoles (61a, b; 62a-c; 63; 64a-d; 65b-d) and 5-[2-(azepan-1-yl)ethoxy]-1*H*-indole (65e)

The amine (**12a**, piperidine, **7a**, pyrrolidine or azepane, 3 eq), Cs_2CO_3 (4 eq) and the 3-chloropropoxyindole (**60b-d**) / 5-(2-chloroethoxy) indole **60e** (1 eq) in MeCN (5 – 10 mL) was refluxed with stirring for 24-48 h and cooled to RT on completion. The solvent was removed under vacuum, the residue extracted with DCM (3 x 10 mL) and worked up in the usual way. The crude product was purified by column chromatography (DCM: methanol, 30: 1) to give the desired products (**61a, b; 62a – c; 63; 64 a – e; 65b – e**) in yields ranging from 15 to 53 %.

4-[2-(Azepan-1-yl)propoxy]-1*H*-indole (65a)

Potassium iodide (KI, 236 mg, 1.42 mmol) was added to a solution of 4-(3-chloropropoxy)-1*H*-indole (**60a**) (150 mg, 0.71 mmol) in MeCN (10 mL). The reaction mixture was heated to reflux for 30-45 min, then cooled to RT, followed by addition of azepane (240 µL, 2.13 mmol) and K_2CO_3 (392 mg, 2.84 mmol). Heating was resumed for another 24 to 48 h. The reaction was monitored by TLC (DCM: MeOH, 5: 1), and on completion, cooled to RT, extracted with DCM (3 x 10 mL) and worked up in the usual way. The crude residue was purified by column chromatography (DCM: methanol, 30: 1) to give the desired product (**65a**) as a yellow semi-solid in 34 % yield. ^{1}H NMR (400 MHz, $CDCl_3$) δ 8.69 (s, br, 1H), 7.15 – 7.05 (m, 2H), 7.00 (d, *J* = 8.2 Hz, 1H), 6.67 (ddd, *J* = 0.8, 2.1, 3.0 Hz, 1H), 6.53 (d, *J* = 7.6 Hz, 1H), 4.17 (t, *J* = 6.3 Hz, 2H), 2.83 – 2.68 (m, 6H), 2.15 – 2.03 (m, 2H), 1.77 – 1.57 (m, 8H); MS (ESI): Calculated for $C_{17}H_{24}N_2O$ 272.19, found 273.15 $[M+H]^+$.

Bacterial strains and culture conditions. *Mycobacterium bovis* BCG (ATCC 35734) and *Mycobacterium tuberculosis* H37Rv (*Mtb,* ATCC 27294) were grown in complete Middlebrook 7H9 medium (BD Difco, Detroit, Michigan) supplemented with 0.05% (v/v) Tween-80 (Sigma-Aldrich), 0.5% (v/v) glycerol (Fisher Scientific), and 10% (v/v) Middlebrook albumin−dextrose−catalase (BD Difco). To determine if MIC values were subjected to a serum or glycerol shift, Middlebrook 7H9 broth was supplemented with 10% fetal bovine serum or prepared without glycerol.

Colony forming unit (CFU) enumeration CFU enumeration of *M. bovis* BCG was performed by plating 10 µL of appropriate dilutions of cultures onto each well of a 12-well plate containing Middlebrook 7H10 agar supplemented with 0.5% (v/v) glycerol and 10% (v/v) oleic acid−albumin− dextrose−catalase (OADC, BD Difco). CFU counting of *Mtb* H37Rv was carried out by dividing each petri dish into two equal parts and then plating 50 µL of appropriate dilutions of cultures onto each part of the dish containing Middlebrook 7H10 agar.

Minimum inhibitory concentration (MIC) determination MICs were determined on *M. bovis* BCG and *Mtb* H37Rv using the broth dilution method as described earlier. [11]

Minimum Bactericidal Concentration (MBC) determination MBC in *M. bovis* BCG was determined by CFU enumeration on Middlebrook 7H10 agar plates using 12-well plates after exposure to a given concentration of test compound. Bacterial cultures were grown to mid-log phase, adjusted to a final OD_{600} = 0.05 (approximately 5 x 10^6 CFU/mL) and then treated with 0.5 x, 1x, 2x or 4x MIC_{90} of test compound for 5 days at 37˚C, 110 rpm. Drug-free cultures were plated at the start of the experiment to determine the bacterial load of the inoculum. After incubation (5 days), the compound-treated cultures were plated to determine CFUs. The same procedure was followed for *Mtb* H37Rv except that cultures were exposed to test compound for 7days at 37˚C, 80 rpm. MBC_{90}, MBC_{99} and $MBC_{99.9}$ are defined as the concentrations required to reduce CFU by 10, 100 and 1000-fold respectively as compared to the untreated inoculum at time point zero.

Loebicidal Concentration (LCC) The method of Gengenbacher *et al.* was followed. [35] Briefly, *Mtb* H37Rv was grown in 1 L roller bottle containing complete 7H9 broth at 37°C, 2 rpm. Mid-log phase bacilli at OD_{600} = 0.4 - 0.6 were spun down and washed three times with 1 x PBS (Invitrogen, Life Technologies) supplemented with 0.025 % Tween-80 and diluted to a final OD_{600} of 0.1. 50 mL of this suspension was transferred into a 1 L roller bottle and starved for 14 days at 37 °C, 2 rpm. The bactericidal activity of **12** or **13** against nutrient-starved non-growing bacilli was determined by exposing 1 mL of OD_{600} = 0.05 culture to various concentrations of

test compound in round-bottom 14 mL snap-cap tubes at 37 °C, 80 rpm for 7 days. CFU was determined by plating appropriate dilutions of the cultures on Middlebrook 7H10 agar. LCC_{90}, LCC_{99} and $LCC_{99.9}$ of test compound are defined as the Loebicidal concentrations required to bring about 10, 100 and 1000-fold reduction in CFU respectively as compared to the drug free inoculum at time point zero.

Spontaneous resistant mutant selection Mutant selection in *M. bovis* BCG was carried out by plating 10^6 - 10^9 CFU/mL of mid-log-phase pre-cultures on Middlebrook 7H10 agar plates containing 2 x, 4 x and 8 x MIC_{90} of **12** or **71**. Plates were incubated at 37°C for 8 weeks. Colonies were picked from selection plates and re-streaked on agar containing the same concentration of **12** or **71** for colony purification and to verify drug resistance.

Mtb H37Rv resistant mutants were isolated by plating CFU (10^7 - 10^9) from mid-log phase pre-cultures on Middlebrook 7H10 agar plates containing 2 x, 4 x and 8 x MIC_{90} of **12.** To select **71** - resistant *Mtb* mutants, 10^8 and 10^9 CFU/mL of mid-log phase *Mtb* H37Rv pre-cultures were plated onto Middlebrook 7H10 agar containing 1x, 2 x and 4 x MIC_{90} of **71**. Plates were incubated at 37°C for 8 weeks. Colonies were picked from selection plates and re-streaked on agar containing the same concentration of **12** or **71** for colony purification and to verify drug resistance.

Cytotoxicity determinations Vero E6 cells. Cytotoxicity determinations on the African green monkey kidney epithelial cells (48 h) were carried out as previously reported. [11]

Compound-induced hemolysis of Human Red Blood Cells. Test compounds were tested at various concentrations for hemolysis of human red blood cells (37 ^oC, 1 h, phosphate buffered saline) as described previously. [11] The procedure for collection of blood from donors was approved by the Institutional Review Board of the National University of Singapore.

Differential Scanning Calorimetry (DSC) DSC was employed to determine the effects of selected compounds on DMPG multilamellar vesicles as previously described. [10]

Membrane Permeability Determination Mid-log-phase *M. bovis* BCG cultures at OD_{600} = 0.1 in complete 7H9 broth were treated with 4-fold MIC_{90} concentrations of test compounds. Negative control was isoniazid tested at 3.2 μM. At each time point, sufficient volumes of cultures were washed twice and re-suspended into 500 μL of 0.9 % NaCl at OD_{600} = 0.5. Each 500 μL of sample was incubated with 0.75 μL of SYTO 9 (3.3 mM, Molecular Probes, Invitrogen) and 0.75μL of propidium iodide (PI, 20 mM, Molecular Probes, Invitrogen) in the dark at 37 ºC for 15 min. Dye-treated cultures were spun down, re-suspended in 500 μL of 0.9 % NaCl and dispensed into flat-bottomed 96-well black plates (200 μL/well). Green and red fluorescence were recorded at λ_{ex} = 488 nm/ λ_{em} = 530 nm and λ_{ex} = 488 nm/ λ_{em} = 630 nm respectively, using Tecan Infinite M200 PRO plate reader. In this assay, the green/red (G/R) fluorescence ratio of drug-free (DF) cultures at each time point was assumed to represent 0% membrane permeabilization and the G/R ratio of 5% (v/v) SDS-treated culture was used to indicate 100% membrane permeabilization. % Membrane permeabilization of drug-treated culture at each time point was calculated as follows:

$$\frac{G/R\ ratio\ of\ DF\ culture - G/R\ ratio\ of\ drug\ treated\ culture}{(G/R\ ratio\ of\ DF\ culture\ - G/R\ ratio\ of\ 5\%\ SDS\ treated\ culture)/100}$$

To correlate changes in membrane permeability to cell viability, the time-kill curves of drug-treated cultures were concurrently monitored by plating diluted cultures on Middlebrook 7H10 agar in 12-well plates for CFU enumeration. Experiments were performed in three independent biological replicates.

p*iniBAC* Cell Envelope Stress Reporter System Compounds **1,12,13** and isoniazid (0.4 - 100 μM) were incubated with recombinant *M. bovis*-p*iniBAC*-RFP strain for 24 h to assess their effects on envelope-stress associated promoter activity following a previously described method. [11]

Determination of Membrane Potential. Membrane potential of treated *M. bovis* BCG cultures harvested at mid-log phase, and adjusted to OD_{600} = 0.1 in complete 7H9 medium with test

compound (**1, 12, 13, 71**) at 4-fold MIC_{90}, were measured using the *Bac*light™ Bacterial Membrane Potential Kit (Life Technologies, CA, USA) as described in an earlier report. [11]

Solubility Determinations. Solubility determinations were carried out on Multiscreen Solubility filter plates (Millipore- MSSLBPC10) from Millipore Corporation (MA, USA) following the protocol (PC2445EN00) from the manufacturer.

PAMPA Pe Determinations Determinations were carried out on MultiScreen-IP PAMPA assay (donor) plates (MAIPNTR10) and MultiScreen Receiver Plates (MATRNPS50) from Millipore Corporation (USA) with 1 % lecithin (Sigma Aldrich, USA) in dodecane (Reagent Plus®, Sigma Aldrich USA) as the lipid barrier. Pe was determined following the method described by Ramanujulu *et al*. [36]

Microsomal Stability. Compounds **1, 12** and **13** were incubated with male rat liver microsomes over 45 min at 37°C for the determination of microsomal stability. Details are given in SI.

Determination of Michael acceptor reactivity by NMR The method described by Avonto *et al* was followed with some modifications. [27] The ^{1}H NMR spectrum of **12** (0.05 mmol) was recorded in DMSO-d_6 (0.5 mL) and deuterated acetic acid (5 µL, 1% v/v). To the same sample in a tightly capped Eppendorf tube was added cysteamine (0.5 mmol, Sigma-Aldrich, USA), sonicated for 10 min, and quickly transferred to an NMR tube for the recording of the spectrum. The ^{1}H NMR spectrum of the same sample was collected again after 30 min and 24 h of standing at RT. ^{1}H NMR spectra were analyzed using Mnova 10.0.2 (Mestrelab Research, CA, USA). The same procedure was followed to determine the reactivity of **13** to cysteamine.

Animals and ethics assurance. Mouse studies were carried out in accordance with the Guide for the Care and Use of Laboratory Animals of the National Institutes of Health, with approval from the Institutional Animal Care and Use Committee of the New Jersey Medical School, Newark (CD-1 mice), National University of Singapore's Institutional Animal Care and Use Committee (BALB/c mice). All animals were maintained under specific pathogen-free conditions

and fed water and chow ad libitum, and all efforts were made to minimize suffering or discomfort. Studies in *M. tuberculosis* infected animals were performed in Biosafety Level 3 facilities approved for the containment of *M. tuberculosis*.

Pharmacokinetic (PK) analyses. Snapshot PK studies were performed in uninfected CD-1 mice after single dose of 25 mg/kg via the oral route (p.o.), as described previously. [37] The p.o. formulation was dosed as a solution consisting of of 5%DMA / 65% PEG300 (polyethylene glycol) / 30% D5W (dextrose 5% in sterile water). Blood was collected at 30 min, 1, 3, and 5h post dose. Plasma was obtained by centrifugation for 10 min at 5,000 rpm and stored at -80°C until analyzed. Lungs were collected at the final time point (5h), weighed and homogenized in approximately 5 volumes of PBS, and stored at -80C until analyzed. Concentrations of **1, 12,** and **13** were measured as described below. The PK parameters (area under the curve [AUC_{0-t} and AUC_{0-24}], peak plasma concentration [C_{max}], half-life [$t_{1/2}$], and elimination rate constant [k_{el}]) were calculated from mean concentrations using Microsoft Excel (Office 2010; Microsoft Corp., Redmond, WA).

Analytical Methods. A neat 1mg/mL DMSO stock solution of test compound was first serially diluted in 50/50 acetonitrile water and subsequently serially diluted in drug-free CD1 mouse plasma (K_2EDTA, Bioreclamation IVT, NY) to create standard curves and quality control (QC) spiking solutions. 20 µL of standards, QC samples, control plasma, and study samples were extracted by adding 200 µL of acetonitrile/methanol 50/50 protein precipitation solvent containing the internal standard (10 ng/mL verapamil). Extracts were vortexed for 5 minutes and centrifuged at 4000 RPM for 5 minutes. 100 µL of supernatant was transferred for HPLC coupled to tandem mass spectrometry (LC/MS-MS) analysis and diluted with 100 µL of Milli-Q deionized water.

LC/MS-MS quantitative analysis was performed on a AB Sciex Qtrap 6500+ triple-quadrupole mass spectrometer coupled to a Shimadzu 30ACMP HPLC system, and chromatography was performed on an Agilent Zorbax SB-C8 column (2.1x30 mm; particle size, 3.5 µm) using a

reverse phase gradient elution. Milli-Q deionized water with 0.1% formic acid was used for the aqueous mobile phase and 0.1% formic acid in acetonitrile for the organic mobile phase. Multiple-reaction monitoring of parent/daughter transitions in electrospray positive-ionization mode was used to quantify all molecules. Data processing was performed using Analyst software (Version 1.6.2; Applied Biosystems Sciex).

Animal tolerability and efficacy experiments. Eight to ten week old female BALB/c mice were maintained in groups of 3 or 4 in individually ventilated cages under specific pathogen free conditions at the National University of Singapore Biosafety Level 3 Core Facility. Food and water were offered *ad libitum*. Test compounds (**1, 12**) were formulated in equal volumes of polyethylene glycol 400 and 5% glucose and administered at a dose of 100 mg/kg in a volume of 200 µL by oral gavage. Acute toxicity was assessed by dosing groups of 3 mice on three consecutive days followed by a monitoring period of 7 days. Animals were subsequently euthanized by CO_2 to assess gross pathological changes. For *in vivo* efficacy determination, mice were infected with 100-200 CFU *M. tuberculosis* H37Rv using a full body inhalation exposure system (GlasCol). After 14 days, drug treatment was initiated for 6 days per week for 4 weeks. Isoniazid at a dose of 25 mg/kg formulated in 0.25% methyl cellulose served as control. Mice were euthanized at designated time points by CO_2. Bacterial burden of organs was determined by plating serial dilutions of organ homogenates onto Middlebrook 7H11 agar supplemented with 20 µg/mL ampicillin and 10 µg/mL cycloheximide. Colonies were counted after 3 - 4 weeks of incubation at 37 °C.

Acknowledgements

This research was supported by the Republic of Singapore Ministry of Education Academic Research Fund R148000234114 to GML and Ministry of Health National Medical Research Council under its TCR Flagship grant NMRC/TCR/011-NUHS/2014 and Centre Grant “MINE”, Research Core #4 NMRC/CG/013/2013 to TD. The TCR Flagship grant and Centre Grant are part of the Singapore Programme of Research Investigating New Approaches to Treatment of

Tuberculosis (SPRINT-TB; www.sprinttb.org) managed by Pauline Yoong and led by Nick Paton. TD holds a Toh Chin Chye Visiting Professorship at the Department of Microbiology and Immunology, Yong Loo Lin School of Medicine, National University of Singapore. Research reported in this publication is also supported by the National Institute of Allergy and Infectious Diseases of the National Institutes of Health under Award Number R01AI132374 and by the Cystic Fibrosis Foundation under Award Number DICK17XX00 to TD. The content is solely the responsibility of the authors and does not necessarily represent the official views of the National Institutes of Health or the Cystic Fibrosis Foundation. LM and SAN gratefully acknowledge graduate scholarships from Ministry of Education, Singapore. We thank Jian Liang Low for laboratory management. Our appreciation goes to Dr David Alland, Rutgers New Jersey Medical School for providing the p*ini*BAC reporter plasmid, Dr Yoshiyuki Yamada, National University of Singapore for providing a modified version of the reporter p*ini*BAC-RFP and Dr R. Manjunatha Kini, National University of Singapore for providing human blood for the hemolysis assay.

Supporting Information Available

Spectral data of synthesized intermediates and final compounds; Purity data of final compounds; ^{1}H NMR spectra of **6** and **65a**; ^{1}H NMR, ^{13}C NMR, HRMS and HPLC spectra of **12, 13;** Scheme for synthesis of **52** and **53;** Loebicidal activities of **12** and **13** against *Mtb* H37Rv; Structure and antimycobacterial profile of **71;** Membrane depolarization of *M. bovis* BCG cultures by **1** and **71;** Electrophilic reactivity of **13** to cysteamine as evaluated by ^{1}H NMR; Protocol for microsomal stability determinations; Molecular Formula Strings of final compounds. This material is available via the Internet at http://pubs.acs.org.

Abbreviations

BCG, Bacillus Calmette-Guerin; CFU, colony forming unit; $DiOC_2$, 3,3-diethyloxacarbocyanine iodide; DMPG, 2-dimyristolyl-*sn*-glycero-3-phosphatidylglycerol; DprE1, decaprenylphosphoryl-

beta-D-ribose oxidase; DSC, differential scanning calorimetry; log P, logarithm to base 10 of partition coefficient P; MIC, Minimum inhibitory concentration; MBC, Minimum bactericidal concentration; MtB, *Mycobacterium tuberculosis*; PI, propidium iodide; RFP, red fluorescent protein; SI, Selective Index; TB, tuberculosis.

Conflict of Interest Declaration

The authors declare no competing financial interest.

Corresponding Authors Information

Thomas Dick, Email td367@njms.rutgers.edu; Tel : 973- 854-3220

Mei-Lin Go; Email phagoml@nus.edu.sg; Tel: +65-65162654.

References

1. Daniel, T.M. The History of Tuberculosis. *Resp. Med.* **2006**, *100*, 1862-1870.

2. World Health Organization. Global Tuberculosis Report 2017. WHO Press: France, 2017.

3. Dheda, K.; Limberis, J.D.; Pietersen, E.; Phelan, J.; Esmail, A.; Lesosky, M.; Fennelly, K.P.; Te Riele, J.; Mastrapa, B.; Streicher, E.M.; Dolby, T.; Abdallah, A.M.; Ben-Rached, F.; Simpson, J.; Smith, L.; Gumbo, T.; van Helden, P.; Sirgel, F.A.; McNerney, R.; Theron, G.; Pain, A.; Clark, T.G.; Warren, R.M. Outcomes, Infectiousness, and Transmission Dynamics of Patients with Extensively Drug-Resistant Tuberculosis and Home-Discharged Patients with Programmatically Incurable Tuberculosis: A Prospective Cohort Study. *Lancet Respiratory Med* **2017***, 5,* 269-281

4. Working Group on New TB drugs. https://www.newtbdrugs.org/pipeline/clinical

5. Hurdle, J. G; O'Neill, A. J.; Chopra, I.; Lee, R. E. Targeting Bacterial Membrane Function: An Underexploited Mechanism for Treating Persistent Infections. *Nat. Rev*. *Microbiol*. **2011**, *9*, 62-75.

6. Chen, C.; Gardete, S.; Jansen, R.S.; Shetty, A.; Dick, T.; Dartois, V. Verapamil Targets Membrane Energetics in *Mycobacterium tuberculosis*. *Antimicrob. Agents Chemother*. **2018**, *62*, e02107 - 02117.

7. Moreira, W.; Aziz, D.; Dick, T. Boromycin Kills Mycobacterial Persisters without Detectable Resistance. *Front. Microbiol.* **2016,** *7,* Article 199.

8. Koh, J.J.; Zou, H.; Mukherjee, D.; Lin, S.; Lim, F.; Tan, J.K.; Tan, D.Z.; Stocker, B.L.; Timmer, M.S.M.; Corkran, H.M.; Lakshminarayanan, R.; Tan, D.T.H.; Cao, D.; Beuerman, R.W.; Dick, T.; Liu, S. Amphiphilic Xanthones as a Potent Chemical Entity of Anti-microbial Agents with Membrane-Targeting Properties. *Eur. J. Med. Chem.* **2016**, *123*, 684-703.

9. Dunn, E.A.; Roxburgh, M.; Larsen, L.; Smith, R.A.J.; McLellan, A.D.; Heikal, A.; Murphy, M.P.; Cook, G.M. Incorporation of Triphenylphosphonium Functionality Improves the Inhibitory Properties of Phenothiazine Derivatives in *Mycobacterium tuberculosis*. *Bioorg. Med. Chem.* **2014,** *22,* 5320-5328.

10. Yang, T.M.; Moreira, W.; Nyantakyi, S.A.; Chen, H.; Aziz, D.; Go, M.L.; Dick, T. Amphiphilic Indole Derivatives as Antimycobacterial Agents: Structure-Activity Relationships and Membrane Targeting Properties. *J. Med. Chem*. **2017**, *60*, 2745-2763.

11. Li, M.; Nyantakyi, S.A.; Gopal, P.; Aziz, D.B.; Dick, T.; Go, M.L. Indolylalkyltriphenyl-phosphonium Analogues are Membrane-Depolarizing Mycobacterial Agents. *ACS Med. Chem. Lett.* **2017,** *8*, 1165-1170.

12. Makarov, V.; Manina, G.; Mikusova, K.; Mollmann, U.; Ryabova, O.; Saint-Joanis, B.; Dhar, N.; Pasca, M.R.; Buroni, S.; Lucarelli, A.P.; Milano, A.; De Rossi, E.; Belanova, M.; Bobovska, A.; Dianiskova, P.; Kordulakova, J.; Sala, C.; Fullam, E.; Schneider, P.; McKinney, J.D.; Brodin, P.; Christophe, T.; Waddell, S.; Butcher, P.; Albrethsen, J.; Rosenkrands, I.; Brosch, R.; Nandi, V.; Bharath, S.; Gaonkar, S.; Shandil, R.K.; Balasubramanian, V.; Balganesh, T.; Tyagi, S.; Grosset, J.; Riccardi, G.; Cole, S.T. Benzathiazinones kill *Mycobacterium tuberculosis* by Blocking Arabinan Synthesis. *Science* **2009,** *324*, 801-804.

13. Trefzer, C.; Rengifo-Gonzalez, M.; Hinner, M.J.; Schneider, P.; Makarov, V.; Cole, S.T.; Johnsson, K. Benzothiazinones: Prodrugs that Covalently Modify the Decaprenylphosphoryl-

beta-D-ribofuranose 2'-epimerase DprE1 of *Mycobacterium tuberculosis*. *J. Am. Chem. Soc.* **2010,** *132*, 13663-13665.

14. Trefzer, C.; Skovierova, H.; Buroni, S.; Bobovska, A.; Nenci, S.; Molteni, E.; Pojer, F.; Pasca, M.R.; Makarov, V.; Cole, S.T.; Riccardi, G.; Mikusova, K.; Johnsson, K. Benzothiazinones are Suicide Inhibitors of Mycobacterial Decaprenylphosphoyrl-beta-D-ribofuranose 2'-oxidase DprE1. *J. Am. Chem. Soc.* **2010,** *134*, 912-915.

15. Makarov, V.; Lechartier, B.; Zhang, M.; Neres, J.; van der Sar, A.M.; Raadsen, S.A.; Hartkoorn, R.C.; Ryabova, O.B.; Vocat, A.; Decosterd, L.A.; Widmer, N.; Buclin, T.; Bitter, W.; Andries, K.; Pojer, F.; Dyson, P.J.; Cole, S.T. Towards a New Combination Therapy for Tuberculosis with Next Generation Benzothiazinones. *EMBO Mol. Med.* **2014,** *6*, 372-383.

16. Gao, C.; Ye, T.; Wang, N.; Zeng, X.; Zhang, L.; Xiong, Y.; You, X.; Xia, Y.; Xu, Y.; Peng, C.; Zuo, W.; Wei, Y.; Yu, L. Synthesis and Structure-Activity Relationships Evaluation of Benzothiazinone Derivatives as Potential Anti-tubercular Agents. *Bioorg. Med. Chem. Lett.* **2013,** *23,* 4919-4922.

17. Zheng Y.; Tice, C.M.; Singh, S.B. The Use of Spirocyclic Scaffolds in Drug Discovery. *Bioorg. Med. Chem. Lett.* **2014,** *24,* 3673-3682.

18. Tai, V.W.F.; Garrido, D.; Price, D.J.; Maynard, A.; Pouliot, J.J.; Xiong, Z.; Seal III, J.W.; Creech, K.L.; Kryn, L.H.; Baughman, T.M.; Peat, A.J. Design and Synthesis of Spirocyclic Sompounds as HCV Replication Inhibitors by Targeting Viral NS4B Protein. *Bioorg. Med. Chem. Lett.* **2014,** *24,* 2288-2294.

19. Whitney, L.; Petrilli, S.B.; Hoyt, C.L.; McMasters, D.; Verras, A.; Struthers, M.; Cully, D.; Wisniewski, T.; Ren, N.; Bopp, C.; Sok, A.; Chen, Q.; Li, Y.; Tung, E.; Tang, W.; Salituro, G.; Knemeyer, I.; Karanam, B.; Clemas, J.; Zhou, G.; Gibson, J.; Shipley, C.A.; MacNeil, D.J.; Duffy, R.; Tata, J.R.; Ujjainwalla, F.; Ali, A.; Xiong, Y. Discovery of Spirocyclic Aldosterone Synthase Inhibitors as Potential Treatments for Resistant Hypertension. *ACS Med. Chem. Lett.* **2017,** *8*, 128-132.

20. Yeaman, M. R.; Yount, N. Y. Mechanisms of Antimicrobial Peptide Action and Resistance. *Pharmacol. Rev.* **2003,** *55,* 27-55.

21. Fischer, W. Lipoteichoic Acid and Lipids in the Membrane of *Staphylococcus aureus*. *Med. Microbiol. Immunol.* **1994,** *183,* 61-76.

22. Lamy-Freund, M.T.; Riske, K. A. The Perculiar Thermo-structural Behavior of the Anionic Lipid DMPG. *Chem. Phys. Lipids*. **2003**, *122,* 19-32.

23. Alland,D.; Steyn, A.J.; Weisbrod, A.J.; Aldrich, K.; Jacobs, W.R. Jr. Characterization of the *Mycobacterium tuberculosis iniBAC* Promoter, a Promoter that Responds to Cell Wall Biosynthesis Inhibition. *J. Bacteriol.* **2000**, *182,* 1802-1811.

24. Boot, M.; van Winden, V.J.C.; Sparrius, M.; van de Weerd, R.; Speer, A.; Ummels, R.; Rustad, T.; Sherman, D.R.; Bitter, W. Cell Envelope Stress in Mycobacteria is Regulated by the Novel Signal Transduction ATPase IniR in Response to Trehalose. *PLoS Genet.* **2017,** *13,* e1007131-

25. Okano, A.; Isley, N.A.; Boger, D.L. Peripheral Modifications of [ψ[CH_2NH]Tpg^4] Vancomycin with Added Synergistic Mechanisms of Action Provide Durable and Potent Antibiotics. *Proc. Natl. Acad. Sci. U. S. A.* **2017,** *114,* E5052-E5061.

26. Baell, J.B.; Holloway, G.A. New Substructure Filters for Removal of Pan Assay Interference Compounds (PAINS) from Screening Libraries and for their Exclusion in Bioassays. *J. Med. Chem*. **2010**, *53*, 2719-2740.

27. Avonto, C.; Taglialatela-Scafati, O.; Pollastro, F.; Minassi, A.; Di Marzo, V.; De Petrocellis, L.; Appendino, G. An NMR Spectroscopic Method to Identify and Classify Thiol-Trapping Agents: Revival of Michael Acceptors for Drug Discovery? *Angew. Chem. Int. Ed*. **2011**, 50, 467-471.

28. Itahara, T.; Ikeda, M.; Sakakibara, T. Alkenylation of 1-Acylindoles with Olefins Bearing Electron-withdrawing Substituents and Palladium Acetate. *J. Chem. Soc., Perkin Trans. 1*, **1983**, 1361-1363.

29. Dai, H.-G.; Li, J.-T.; Li, T.-S. Efficient and Practical Synthesis of Mannich Bases Related to Gramine Mediated by Zinc Chloride. *Synth. Commun.* **2006**, 36, 1829-1835.

30. Miranda, S.; López-Alvarado, P.; Avendaño, C.; Menéndez, J. C. Convenient Synthesis of Highly Functionalized, 3,4-Disubstituted Indole Building Blocks. *Open Org. Chem. J.*, **2007**, 1, 1-12.

31. Wang, Z. Vilsmeier Formylation. In *Comprehensive Organic Name Reactions and Reagents*; John Wiley & Sons, Inc.: Hoboken, NJ, USA, 2010; pp 2872–2879.

32. Abdel-Magid, A. F.; Carson, K. G.; Harris, B. D.; Maryanoff, C. A.; Shah, R. D. Reductive Amination of Aldehydes and Ketones with Sodium Triacetoxyborohydride. Studies on Direct and Indirect Reductive Amination Procedures. *J. Org. Chem.*, **1996**, 61, 3849-3862.

33. Tiwari, R.; Möllmann, U.; Cho, S.; Franzblau, S. G.; Miller, P. A.; Miller, M. J. Design and Syntheses of Anti-Tuberculosis Agents Inspired by BTZ043 Using a Scaffold Simplification Strategy. *ACS Med Chem Lett.,* **2014**, 5, 587-591.

34. Lepri, S.; Buonerba, F.; Goracci, L.; Velilla, I.; Ruzziconi, R.; Schindler, B. D.; Seo, S. M.; Kaatz, G. W.; Cruciani, G. Indole Based Weapons to Fight Antibiotic Resistance: A Structure−Activity Relationship Study. *J. Med. Chem.*, **2016**, 59, 867-891.

35. Gengenbacher, M.; Rao, S.P.; Pethe, K.; Dick, T. Nutrient-starved, Non-replicating *Mycobacterium tuberculosis* Requires Respiration, ATP Synthase and Isocitrate Lyase for Maintenance of ATP Homeostasis and Viability. *Microbiology* **2010,** *156*, 81-87.

36. Ramanujulu, P.M.; Yang, T.M.; Yap, S.Q.; Wong, F.C.; Casey, P.J.; Wang, M.; Go, M.L. Functionalized Indoleamines as Potent, Drug-like Inhibitors of Isoprenylcysteine Carboxyl Methyltransferase (Icmt). *Eur. J. Med. Chem.* **2013**, *63*, 378-386.

37. Zimmerman, M.; Lestner, J.; Prideaux, B.; O'Brien, P.; Dias-Freedman, I.; Chen, C.; Dietzold, J.; Daudelin, I.; Kaya, F.; Blanc, L.; Chen, P.Y.; Park, S.; Salgame, P.; Sarathy, J.; Dartois, V. Ethambutol Partitioning in Tuberculous Pulmonary Lesions Explains Its Clinical Efficacy. *Antimicrob. Agents Chemother*. **2017,** *61*, e00924-17.

Table of Contents Graphic